DYNAMIC BEHAVIOR OF ANGLE-OF-ATTACK VANE ASSEMBLIES

TECHNICAL REPORT AFIT TR 74-8
DECEMBER 1974

JAMES T. KARAM, JR.
CAPTAIN, USAF

UNITED STATES AIR FORCE

AIR UNIVERSITY

AIR FORCE INSTITUTE OF TECHNOLOGY

Wright-Patterson Air Force Base, Ohio

Dynamic Behavior of Angle-of-Attack Vane Assemblies

James T. Karam, Jr., Captain, USAF
Assistant Professor of Aeronautical Engineering
Air Force Institute of Technology

Technical Report AFIT TR 74-8
December 1974

Approved for public release, distribution unlimited

School of Engineering
Air Force Institute of Technology
Wright-Patterson Air Force Base, Ohio 45433

Preface

T his study of what seemed a very simple system turned into a rather involved effort. It started at the request of Mr. Larry Roberts of the 4950th Test Wing, Aeronautical Systems Division, AFSC, Wright-Patterson AFB, Ohio, and benefited from his continued interest and support. Hopefully, others will find the result useful although it unfortunately supported Larry's concern that the vane dynamics and boom motions might have a significant effect on the gust measurements he was attempting to obtain.

The study itself was supported by many others. Of primary assistance was Professor Harold Larsen, Head of the AFIT Aero Design Center, who advised and guided the wind tunnel test efforts and the theoretical aerodynamics. The tests themselves could not have occurred without the aid of several technicians. Dave Grube of the AFIT School Shops produced beautiful hardware from the crudest of sketches. J.R. Shera of the 4950th's Instrumentation Branch assisted throughout in setting up the vane and its associated electronics. Tom Lokai and Scotty Whitt set up and operated the tunnel. I also wish to thank Dr. Shine, Head of the Aero-Mechanical Engineering Department, and the AFIT administration for providing the time which enables faculty to perform independent research on real world Air Force problems. This report documents the results of AFIT Faculty Research Project Number 74-4. However, I accept full responsibility for any errors or omissions.

Table of Contents

Nomenclature

a	distance from pivot axis to mid-chord; fraction of chord; positive aft
A	aspect ratio; $\frac{w^2}{S}$
b	semi-chord; b = c/2; in
B	damping constant
c	chord; in
$C_{\ell\alpha}$	section lift curve slope; $dC_\ell/d\alpha$ where C_ℓ = (Lift per unit span)/qc
$C_{L\alpha}$	wing lift curve slope; $dC_L/d\alpha$ where C_L = Lift/qS
$C_{m\alpha}$	section moment curve slope; $dC_m/d\alpha$ where C_m = (Moment per unit span)/qc^2
$C_{M\alpha}$	wing moment curve slope; $dC_M/d\alpha$ where C_M = Moment/qSc
E	Young's modulus of elasticity; psi
f_n	natural frequency in Hz; $f_n = \omega_n/2\pi$
q	acceleration due to gravity; 386 in/sec^2
$h,\dot{h},\ddot{h}$	transverse displacement, velocity, and acceleration of pivot axis; in, in/sec, in/sec^2; positive down
h_o	magnitude of sinusoidal pivot axis motion; in
I	cross-section area moment of inertia; in^4
j	$\sqrt{-1}$
J	rotary mass moment of inertia; in lb_f sec^2
J'	effective mass moment of inertia of the entire vane assembly; in lb_f sec^2
K	emperical stiction parameter
ℓ	distance from center of pressure to pivot axis; in
L	beam length; in
m	mass; lb_f sec^2/in

min	minimum of the absolute values function; min $(x_1, x_2, \ldots x_n) = x_i$ when $\lvert x_i \rvert < \lvert x_j \rvert$ for $j = 1, 2, \ldots, n$
M	moment; in lb_f
q	dynamic pressure; $q = \frac{1}{2} \rho U^2$; psi
r	distance from counterweight center of mass to pivot axis; in
sgn	sign function; sgn x = +1 if x > 0, 0 if x = 0, -1 if x < 0
S	vane area; in^2
t	vane thickness; in
T	time; sec
U	freestream velocity, usually $U_{eqv} = \sqrt{2q/\rho_o}$; in/sec
Vol	Volume, in^3
w	spanwise width; in
W	loading per unit length; lb_f/in
x	chordwise distance; in; positive aft
z	vertical displacement; in; positive up
$\alpha, \dot{\alpha}, \ddot{\alpha}$	angular displacement, velocity, and acceleration; rad, rad/sec, rad/sec^2; positive clockwise
α_o	initial angular displacement, or angle of attack of deformed vane, or magnitude of sinusoidal angular displacement; rad
ϕ	phase shift of sinusoidal motion; rad
κ	log decrement
μ_D	dry friction coefficient
μ_V	viscous friction coefficient
π	3.14159 ...
ρ	density; $lb_f\ sec^2/in^4$
ρ_o	sea level density of air; $1.08 \cdot 10^{-7}\ lb_f\ sec^2/in^4$
ζ	damping ratio
ω	frequency of sinusoidal oscillation; rad/sec
ω_n	natural frequency; rad/sec

List of Figures and Tables

Abstract

A relatively simple analytic model was developed for predicting the dynamic behavior of angle-of-attack vane assemblies in response to changes in the free stream direction and/or to transverse motions of the vane's pivot axis. Experimental tests of a typical vane were performed in the AFIT five-foot, low subsonic wind tunnel. Comparisons were made of the model's predictions with these tests and with other test results found in the literature. The natural frequencies of the vanes were predicted reasonably well (within about 20 percent) for all airspeeds -- subsonic and supersonic. The chief difficulty was in estimating the center of pressure location for these very low aspect ratio vanes. Viscous and tip effects were not included in the model. The aerodynamic damping was experimentally found to be essentially independent of airspeed as predicted, but the model's estimates were only within a factor of 2 to 3 of the data. It was found that typical aircraft instrumentation boom motions may lead to significant errors in the apparent angle of attack.

Introduction

Recent events in flight tests have generated the need for a verified model of the dynamic behavior of angle-of-attack vanes -- also variously called incidence vanes and wind vanes. The usual assumption that such a vane responds instantaneously to changes only in the aircraft's attitude is no longer acceptable. Dynamic performance flight testing [1] (obtaining useful data continuously rather than going from one quasi-steady condition to another) is being considered to reduce the duration and cost of flight test programs. For this use, one must not only know the response of the vane to quasi-steady aircraft motions [2] but also the vane's dynamic behavior to transient motions [3]. Another common use of these vane assemblies is as meteorological sensors for wind gusts [4,5]. In particular, the 4950th Test Wing at Wright-Patterson AFB, Ohio has been using these vanes in thunderstorm penetration studies. In this use, the aircraft is flying straight and level while the vane is being used to sense small, rapid changes (gusts) in the free stream's velocity. Again, knowledge of the vane's dynamic behavior is essential since it will act as a low pass filter to gusts. Since the vane is usually mounted on a long, somewhat flexible boom when performing gust measurements, the mechanical vibrations of this boom can also lead to changes in vane angular position. These extraneous motions might lead to significant errors in the observed gust velocities since the effects are inseparable. For all these reasons, a study of the dynamic response of angle-of-attack vane (hereafter called wind vane) assemblies was undertaken.

First, a mathematical model of a windvane was developed. Then experimental tests of the vane used by the 4950th Test Wing were run in

the Air Force Institute of Technology (AFIT) five-foot, low subsonic wind tunnel. These results, along with others found in the literature, were compared with the model's predictions. Finally, some comments concerning vane design are included.

Mathematical Model

Figure 1 is a sketch of an idealized wind vane. A "plate" of some geometry is attached by an arm to a pivoting shaft which extends from the aircraft's instrumentation boom. Usually, a counterweight is provided so that the vane assembly is statically balanced. The pivot shaft is usually connected internally to the shaft of some angular position sensor, e.g., a potentiometer, syncro, etc.

Four major types of moments were considered to act on the vane: inertial, aerodynamic, viscous friction, and dry friction. We thus require that

$$M_{inertia} + M_{aero} + M_{viscous} + M_{dry} = 0 \qquad (1)$$

Let's begin with the aerodynamic moments. Unfortunately, there is no simple expression for the aerodynamic moments of a small aspect ratio ($A = w^2/S$) vane which is the most common in use. Instead, let's follow the usual practice for wings and first consider the moments on a two-dimensional ($A = \infty$), rotating, plunging flat plate in an incompressible, inviscid fluid. Figure 2 defines the coordinates and geometry for such a system. A quasi-steady solution (which ignores the effects of trailing vortices) may be found as equation 5-348 in Bisplinghoff, et al [6], i.e.,

$$M_{aero} = \pi\rho b^2 \left[ba\ddot{h} - Ub\left(\tfrac{1}{2}-a\right)\dot{\alpha} - b^2\left(\tfrac{1}{8}+a^2\right)\ddot{\alpha}\right] + 2\pi\rho Ub^2\left(a+\tfrac{1}{2}\right)\left[\dot{h} + U\alpha + b\left(\tfrac{1}{2}-a\right)\dot{\alpha}\right] \qquad (2)$$

Recalling that the center of pressure for a symmetrical two-dimensional airfoil is at the quarter chord ($b/2$) and that the lift curve slope $C_{\ell\alpha} = dC_\ell/d\alpha = 2\pi$, this equation can be written as

$$M_{aero} = -\left(\ell+\frac{b}{2}\right)^2 \pi\rho b^2 \ddot{\alpha} - 2\left[\frac{(2\ell+b)(\ell+b)}{4\ell^2}\frac{\ell}{U}\right]\left[2\pi\rho U^2\ell b\right]\dot{\alpha} - 2\pi\rho U\ell b\left[\dot{h} + \frac{2\ell+b}{4\ell}\frac{b}{U}\ddot{h}\right] \qquad \text{(per unit span)} \qquad (3)$$

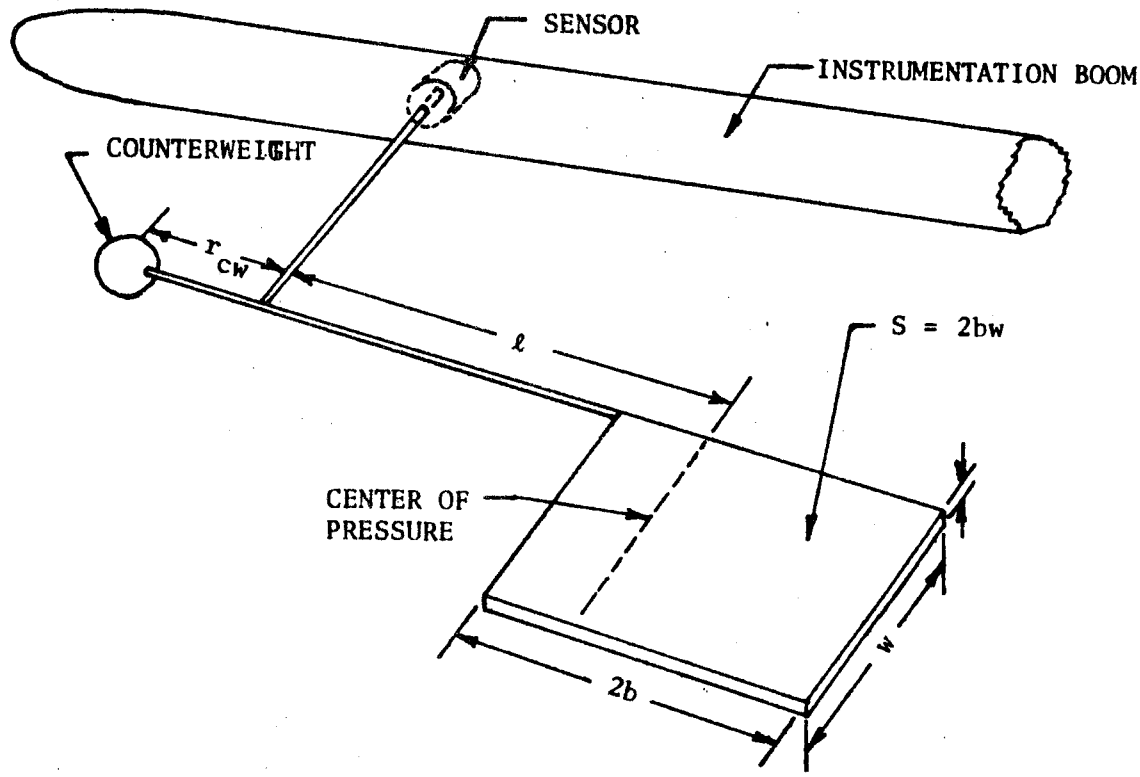

Figure 1 Configuration of an Idealized Wind Vane

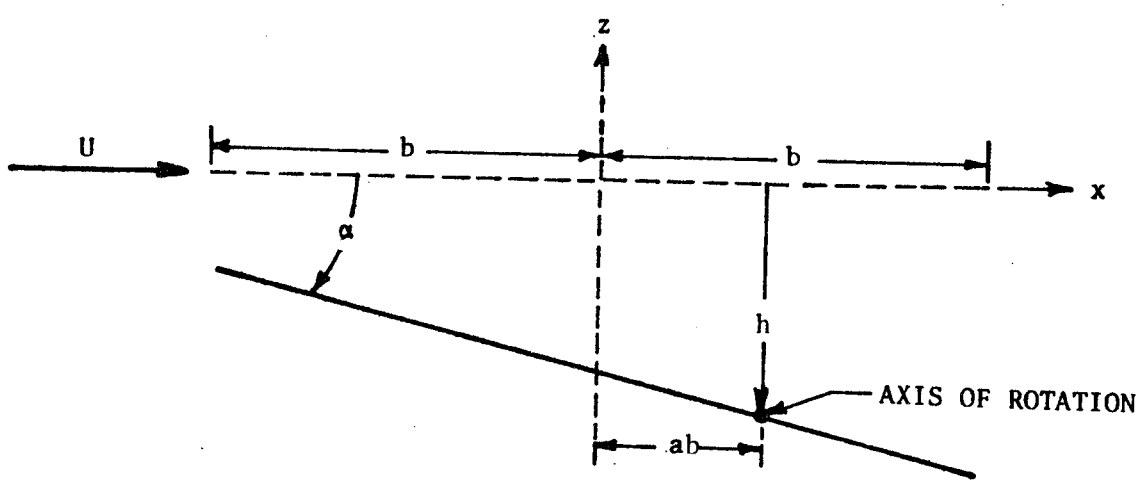

Figure 2 Wind Vane Coordinate System

where ℓ = distance from the pivot axis to the center of pressure $= -(a + \frac{1}{2})b$. This is really the moment per unit span, so if we multiply this equation by the span w and substitute the wing lift slope $C_{L\alpha}$ for the section slope 2π, we obtain

$$M_{aero} = -\left(\ell+\frac{b}{2}\right)^2 \frac{\pi}{2} \rho b S \ddot{\alpha} - 2\left[\frac{(2\ell+b)(\ell+b)}{4\ell^2} \frac{\ell}{U}\right]\left[C_{L\alpha} \ell q S\right] \dot{\alpha} - C_{L\alpha} \ell q S \alpha$$

$$- \frac{C_{L\alpha} \ell q S}{U}\left[\dot{h} + \frac{2\ell+b}{4\ell} \frac{b}{U} \ddot{h}\right] \qquad (4)$$

where S = wing area = 2bw for the assumed rectangular planform.

If the vane is not statically balanced, there will be a static moment. However, its only effect is to change the effective zero angle of attack. This moment has no obvious dynamic effect, but it can move the operating range of the vane into the nonlinear lift regime [7] and thus preclude the use of the simple aerodynamic moment relation just developed in equation 3. Thus, most vanes are statically balanced. For subsequent use, let's note that, for the idealized rectangular vane,

$$M_{static} \cong m_{vane}\left(\ell + \frac{b}{2}\right) - m_{cw}\, r_{cw} = \rho_{vane}\, St\left(\ell + \frac{b}{2}\right) - m_{cw}\, r_{cw} \qquad (5)$$

Frictional forces in bearings, shaftways, and the like will lead to moments of a dissipative nature. Other damping phenomena may result from the air's truly viscous nature (possibly enhanced by perforations or the like [5] or by discrete physical dampers attached to the pivot shaft [8]). In any case, most frictional effects are modeled as a linear, purely viscous damper, i.e.,

$$M_{viscous} = -B_V \dot{\alpha} \qquad (6)$$

where B_V is usually an emperically determined damper constant. Unfortunately, most frictional phenomena for the usual vane construction is really of the dry friction type. Dry friction for rotary motion is

almost impossible to analytically estimate a priori. It may result from sliding shaftways, potentiometer contact drag, bearing friction, or the like. Dry friction is usually idealized as shown in Figure 3a. An increase in the moment needed to initiate motion (sometimes called stiction) is usually noted as in Figure 3b. However, this idealization encounters difficulty in digital simulations because the zero condition cannot be practically obtained. This latter problem leads to numerical instabilities or convergence difficulties. As a practical approximation, something like Figure 3c may be used. Three analytic approximations were used at various times in this study. They were

$$M_{dry} = - B_D \frac{|\alpha| \operatorname{sgn}(\dot{\alpha})}{1+K_1|\dot{\alpha}|} \text{ or } M_{dry} = - B_D \frac{K_2\dot{\alpha}}{1+K_3\dot{\alpha}^2} \text{ or } M_{dry} = - B_D \begin{cases} K_4\dot{\alpha} \text{ if } |\dot{\alpha}| \leq 1/K_4 \\ \operatorname{sgn} \dot{\alpha} \text{ otherwise} \end{cases} \quad (7)$$

The last moment to be considered is the so called inertial torque or moment

$$M_{inertia} = - J\ddot{\alpha} \quad (8)$$

where the mass rotary moment of inertia, J, for the idealized rectangular vane is approximately

$$J_{vane} \simeq m_{vane} \left(\ell^2+\ell b+\frac{7}{12}b^2\right) + m_{cw}\, r_{cw}^2 = \rho_{vane}\, St\left(\ell^2+\ell b+\frac{7}{12}b^2\right) + m_{cw}\, r_{cw}^2 \quad (9)$$

Substituting these various moments into equation (1), we have

$$-J\ddot{\alpha} - \left(\ell+\frac{b}{2}\right)^2 \frac{\pi}{2} \rho b S\ddot{\alpha} - 2\left[\frac{(2\ell+b)(\ell+b)}{4\ell^2} \frac{\ell}{U}\right](C_{L\alpha}\ell q S)\,\dot{\alpha} - C_{L\alpha}\ell q S\alpha$$

$$- \frac{C_{L\alpha}\ell q S}{U}\left(\dot{h} + \frac{2\ell+b}{4\ell} \frac{b}{U} \ddot{h}\right) - B_V\dot{\alpha} - B_D \min\left(K_4\dot{\alpha}, \operatorname{sgn} \dot{\alpha}\right) = 0 \quad (10)$$

$$\text{or } \ddot{\alpha} + (2\zeta\, \omega_n+\mu_V)\,\dot{\alpha}+\omega_n^2\,\alpha+\mu_D \min\left(K_4\dot{\alpha}, \operatorname{sgn} \dot{\alpha}\right) = - \frac{\omega_n^2}{U}\left(\dot{h} + \frac{2\ell+b}{4\ell} \frac{b}{U} \ddot{h}\right) \quad (11)$$

$$\text{where} \qquad \omega_n = \sqrt{\frac{C_{L\alpha}\ell q S'}{J'}} \quad (12)$$

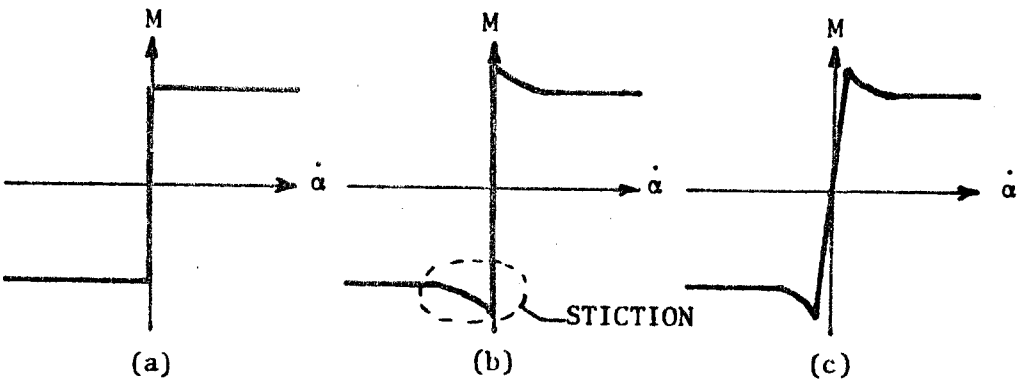

Figure 3 Idealized Dry Friction Models

$$J' = J_{vane} + J_{aero} = J_{vane} + (\ell+\frac{b}{2})^2 \frac{\pi}{2} \rho b S \tag{13}$$

$$\zeta = \frac{(2\ell+b)(\ell+b)}{4\ell^2} \frac{\ell}{U} \omega_n = \frac{(2\ell+b)(\ell+b)}{4\ell} \sqrt{\frac{C_{L\alpha} \ell \rho S}{2J'}} \tag{14}$$

$$\mu_V = \frac{B_V}{J'} \tag{15}$$

$$\mu_D = \frac{B_D}{J'} \tag{16}$$

Usually, $J_{vane} >> J_{aero}$. Further, since this model was based on an incompressible development, if the airspeed U is interpreted as equivalent airspeed, $U_{eqv} = \sqrt{2q/\rho_o}$ where ρ_o = sea level density, then the aerodynamic damping ratio ζ is a constant for a given vane, i.e., independent of airspeed. However, since ω_n increases linearly with airspeed, the aerodynamic damping term, $2 \zeta \omega_n$, increases with airspeed unlike the two friction based terms, μ_V and μ_D, which are simply constants. The friction terms will then only be significant for relatively small airspeeds. Under all these conditions, assuming no impulsive type of pivot axis velocity so that $\ddot{bh}/U$ is not large, the vane model simplifies to

$$\ddot{\alpha} + 2 \zeta \omega_n \dot{\alpha} + \omega_n^2 \alpha = - \omega_n^2 \frac{\dot{h}}{U} \tag{17}$$

where ω_n and ζ are still given by equations 12 and 14 respectively. These simplified equations have previously been developed [2,3] -- at least as the limiting case for

$$\zeta = \frac{\ell}{2} \frac{\omega_n}{U} \text{ when } \ell >> b \tag{18}$$

However, this more complete development will enable a designer or user to quantify the suitability of the simplified model as he can calculate the neglected terms.

Nevertheless, one should caution that even the more complete model given by equation (11) has many inherent simplifications. The obvious ones are that viscous and tip effects are neglected. Further, while the inertial effects of the support and pivot arm may be relatively easily accounted for in calculating or measuring J, aerodynamic forces on these elements are not accounted for. If desired, these forces may be approximated by the potential solution for the moment of a pivoted body of revolution, i.e.,

$$M_{cw \ \& \ support} \simeq 2q \ Vol_{net} \ \alpha \tag{19}$$

where Vol_{net} equals the volume of counterweight and support shaft forward of the pivot minus the volume aft of the pivot. Usually, these volumes are nearly equal so that $Vol_{net} \simeq 0$ or in any case is usually very much less than $C_{L\alpha} \ \ell S$. Note that this approximation ignores the suction peak at the nose usually noted in real air flows. Obviously the vane is assumed rigid. Further, while this was basically a rectangular wing development, we assume that the results will be valid for any planform if the proper $C_{L\alpha}$ and ℓ are used.

Lift curve slope predictions for very small aspect ratio airfoils are best given by Jones' slender body theory [9] as

$$C_{L\alpha} = \pi A/2 \qquad \text{for } A \text{ on the order of 1 or less} \qquad (20)$$

rather than the "lifting line" value cited in most prior articles. While slender body theory was strictly based on long, pointed planforms, its predictions are much more reasonable for any small aspect ratio planform than those provided by "lifting line" type formulas. For non-pointed shapes, one should strictly use a "lifting surface" solution. Nevertheless, for a rectangular planform with an aspect ratio of one, Gersten's lifting surface solution [7] predicts a $C_{L\alpha} = 1.46$.while slender body theory, eqn (20), predicts $C_{L\alpha} = 1.57$ (less than 8% error) and lifting line theory predicts $C_{L\alpha} = 2.09$ (a 43% error). While not usually encountered in aircraft vanes, larger aspect ratios (on the order of 2 to 4) are sometimes used for meteorological vanes. In this case, an all aspect ratio formula may be used, e.g., one due to DeYoung [10]

$$C_{L\alpha} = \frac{2\pi}{1 + \frac{2}{A}\frac{(A + 4)}{(A + 2)}} \qquad (21)$$

Even more difficult is predicting the center of pressure location for small aspect ratios. For rectangular wings, an extrapolation of the results of Table I of Gersten [7] might be used. For other more rounded or pointed shapes, slender body theory [9] predicts a center of pressure at the area centroid of the "effective" planform. On a positive note, slender body theory [9] might also predict that this model is valid for all airspeeds (except possibly transonic) in spite of its incompressible development.

Experimental Program

A wind tunnel test program was conducted on a typical wind vane in the AFIT five foot diameter, low subsonic wind tunnel. This open loop tunnel is capable of providing airspeeds in the test section from 15 to about 200 miles per hour (mph). The vane tested is one which is in current use in thunderstorm penetration studies by the 4950th Test Wing, ASD, AFSC, Wright-Patterson AFB, Ohio. It basically is a 1/16 inch thick fiberglass printed circuit board clad on both sides with 1/32 inch thick balsa sheeting which is linearly tapered to zero thickness at the trailing edge. The vane is attached at the leading edge to a pivot shaft, supported by a ball bearing, which is attached to the rotor of a synchro mounted in the instrumentation boom. Figure 4 is a sketch of the vane geometry. The chord (2b) is about 4 3/4 inches while the span is 2 3/8 inches, so the aspect ratio of the vane is 0.5. The mass rotary moment of inertia of the entire assembly was calculated and experimentally verified to be 0.0012 in lb_f sec^2.

The vane was mounted on the upstream end of the horizontal member of a cruciform mounting assembly. Figure 5 is a photograph of the vane and the supporting cruciform in the tunnel. The geometry of the cruciform upstream horizontal member is identical to that of the actual flight instrumentation boom.

An initial series of tests were run with the cruciform stationary ($\dot{h}\equiv 0$). The vane was set at an initial angle of attack of about 5 degrees and held there by a pin at the base of the pivot shaft. The tunnel was brought up to speed, and then the pin was pulled by means of selonoid connected to the pin by a wire. Figure 6 is a typical oscilloscope trace of the response. Figure 7 is a photograph of the electronics used

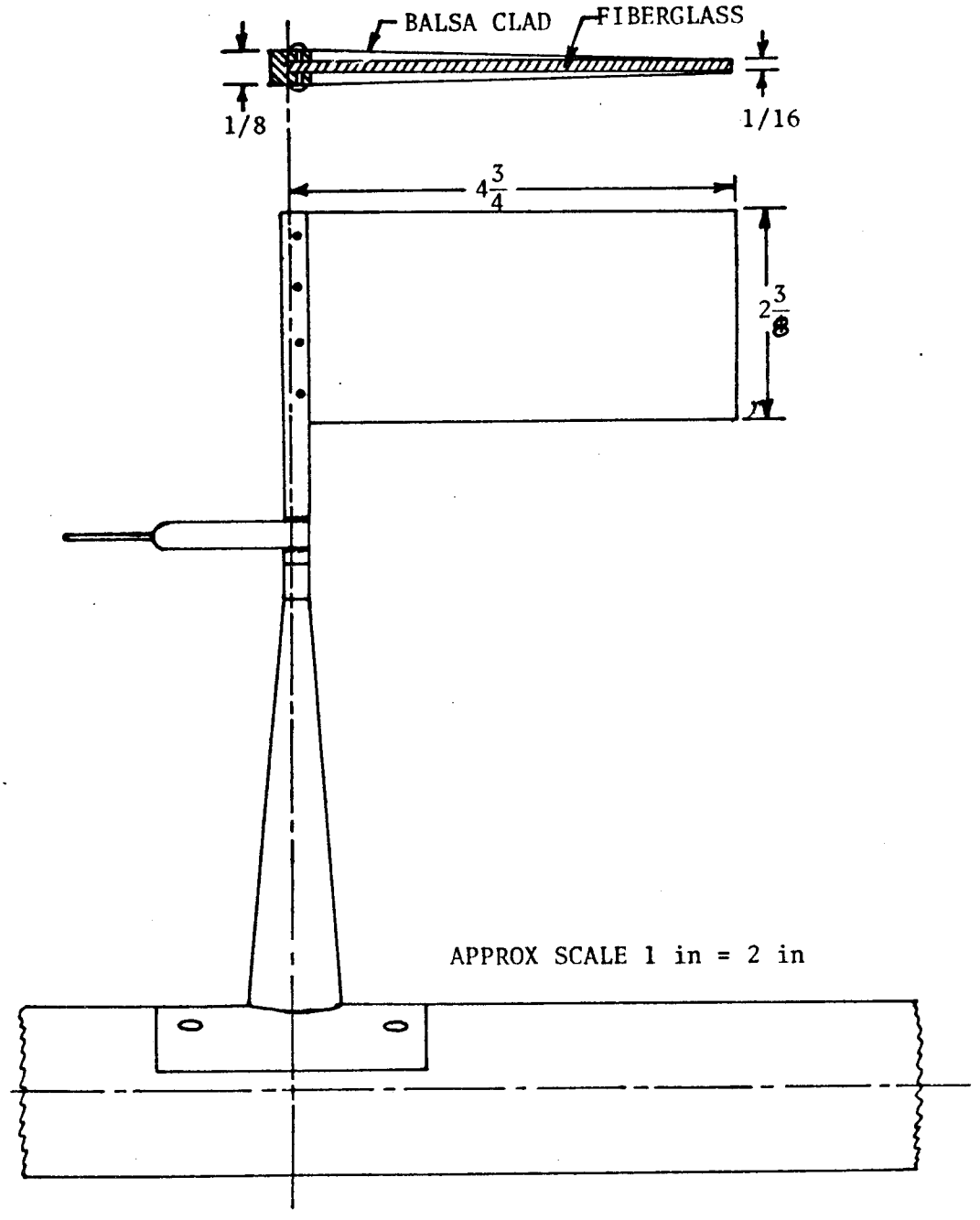

Figure 4 Geometry of Wright-Patterson Vane Assembly

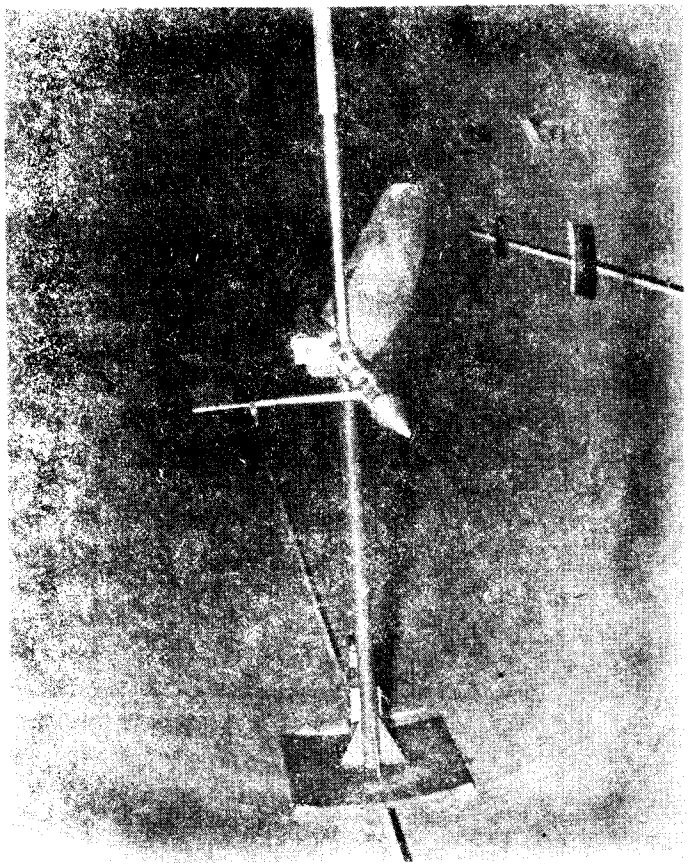

Figure 5 Tunnel Installation of Wright-Patterson Vane

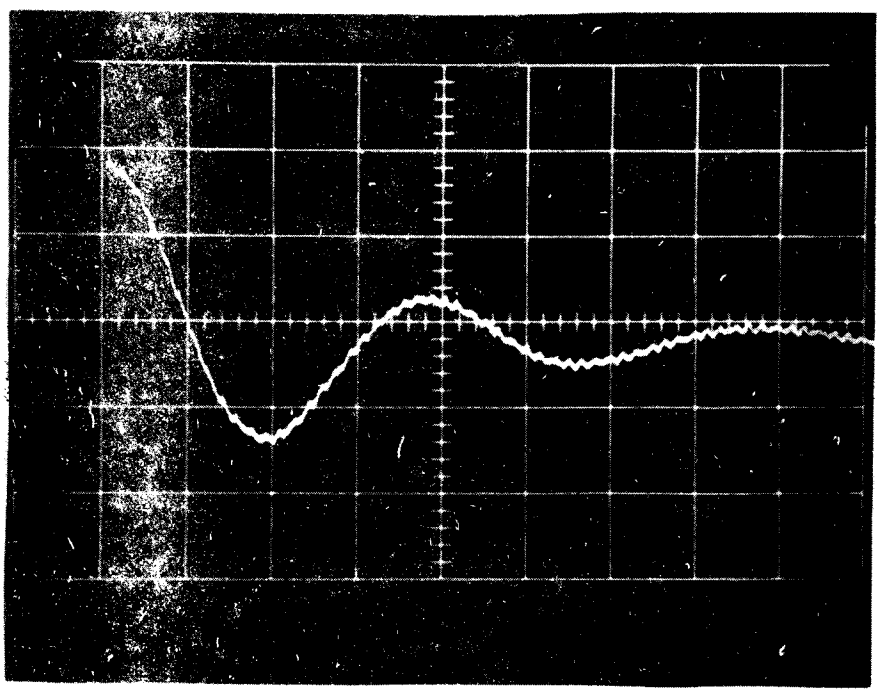

Figure 6 Typical Oscilloscope Trace of a Release from an Initial Angle of Attack Test (see Table I, Run 7)

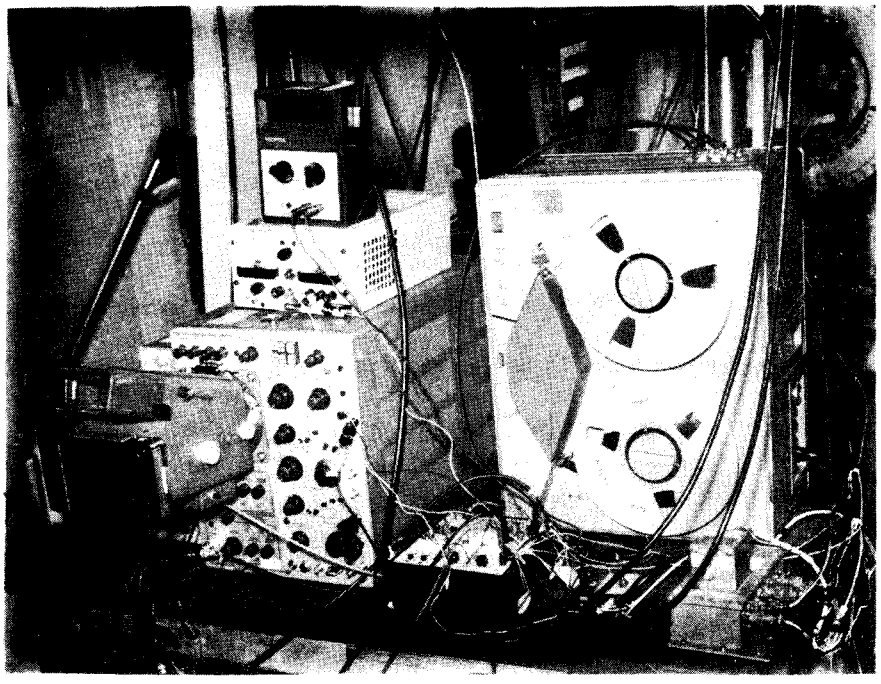

Figure 7 Electronic Monitoring Equipment

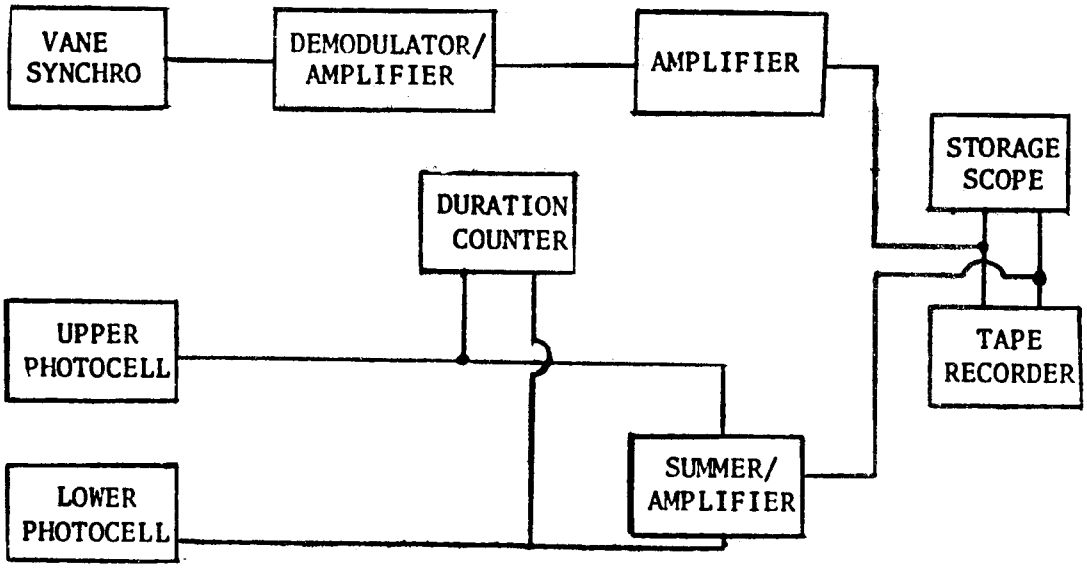

Figure 8 Block Diagram of Test Electronics

to monitor and record the response. Figure 8 is a block diagram of the major electronic components. The observed vane motion was recorded on a storage oscilloscope and a tape recorder.

For the next series of tests, the cruciform's vertical member was connected to an air piston mounted above the tunnel (see Figure 9). The assembly was set about 15 inches above the tunnel centerline, the tunnel was started, and then the piston drove the assembly rapidly back to the center. The interest here was in the response of the vane to motions of its pivot axis. Figure 10 is a typical response for the first few tests. Unfortunately, subsequent tests were characterized by a rapid reversal of angular position on impact. Figure 11 is typical of the subsequent tests. The time history of the cruciform's position was determined for three tests by high-speed photography of the assembly portion which extended through the bottom of the tunnel (see Figure 12). The results of these runs were quite consistent. A typical history is shown as Figure 13. The overall time duration was checked on each run by means of the photoelectric cells shown in Figure 12.

Table I is a summary of all the test data and results. As may be noted, the vane's response was essentially that of a dampened second order system as expected. The effective damping ratio was determined from the log decrement of adjacent extrema, i.e.,

since $$\frac{\alpha_{n+1}}{\alpha_n} = e^{-\zeta\pi/\sqrt{1-\zeta^2}} \tag{22}$$

then $$\zeta = \sqrt{\frac{\kappa^2}{\pi^2+\kappa^2}} \tag{23}$$

where $$\kappa = \ln\left[\frac{\alpha_{n+1}}{\alpha_n}\right] \tag{24}$$

Figure 9 Air Piston Assembly Above the Tunnel

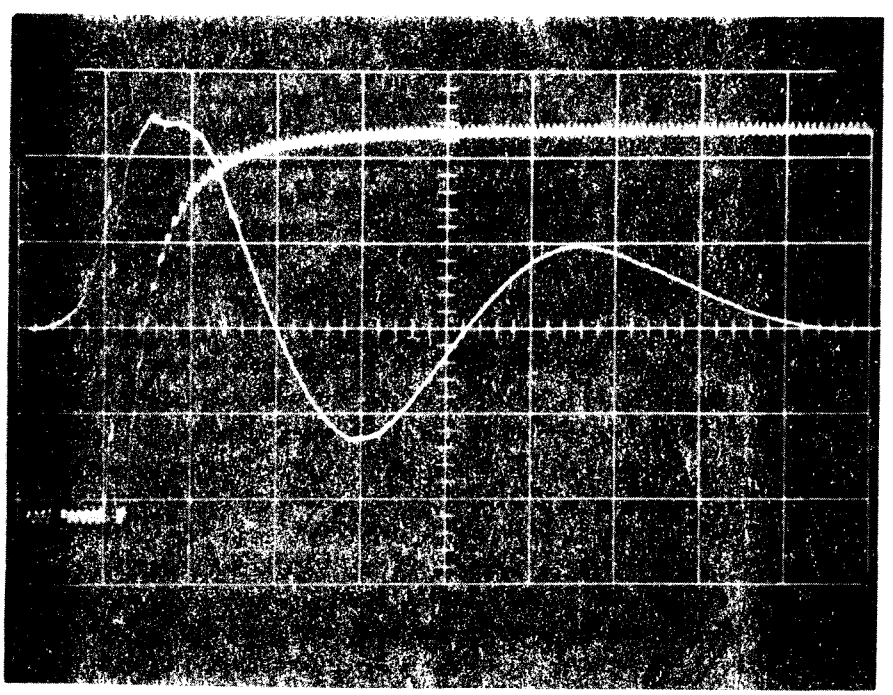

Figure 10 Typical Response of Vane due to Transverse Motion at the Pivot Axis for the First Few Tests (Upper Trace - Angular Position, Lower Trace - Electrical Output)

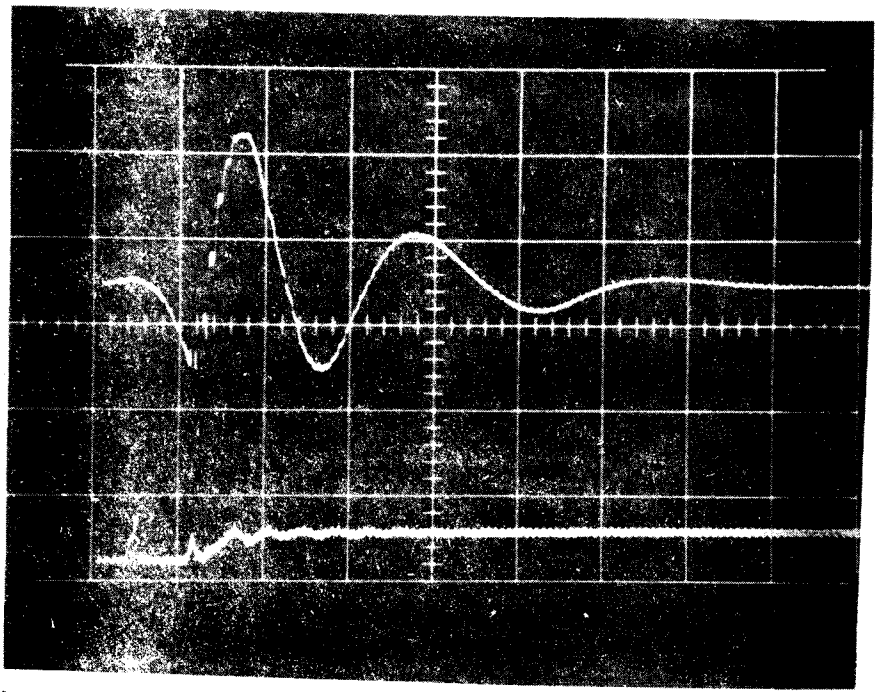

Figure 11 Typical Response of Vane due to Transverse Motions of the Pivot Axis for Remaining Tests (Upper Trace = Angular Position, Lower Trace = Photocell Output, see Table I, Run 21)

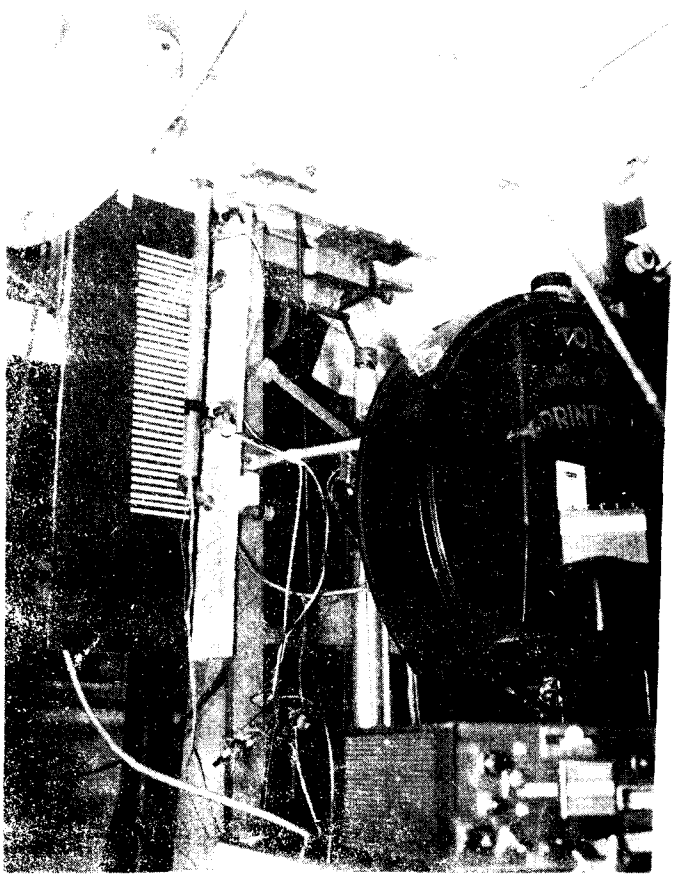

Figure 12 Below Tunnel Installation

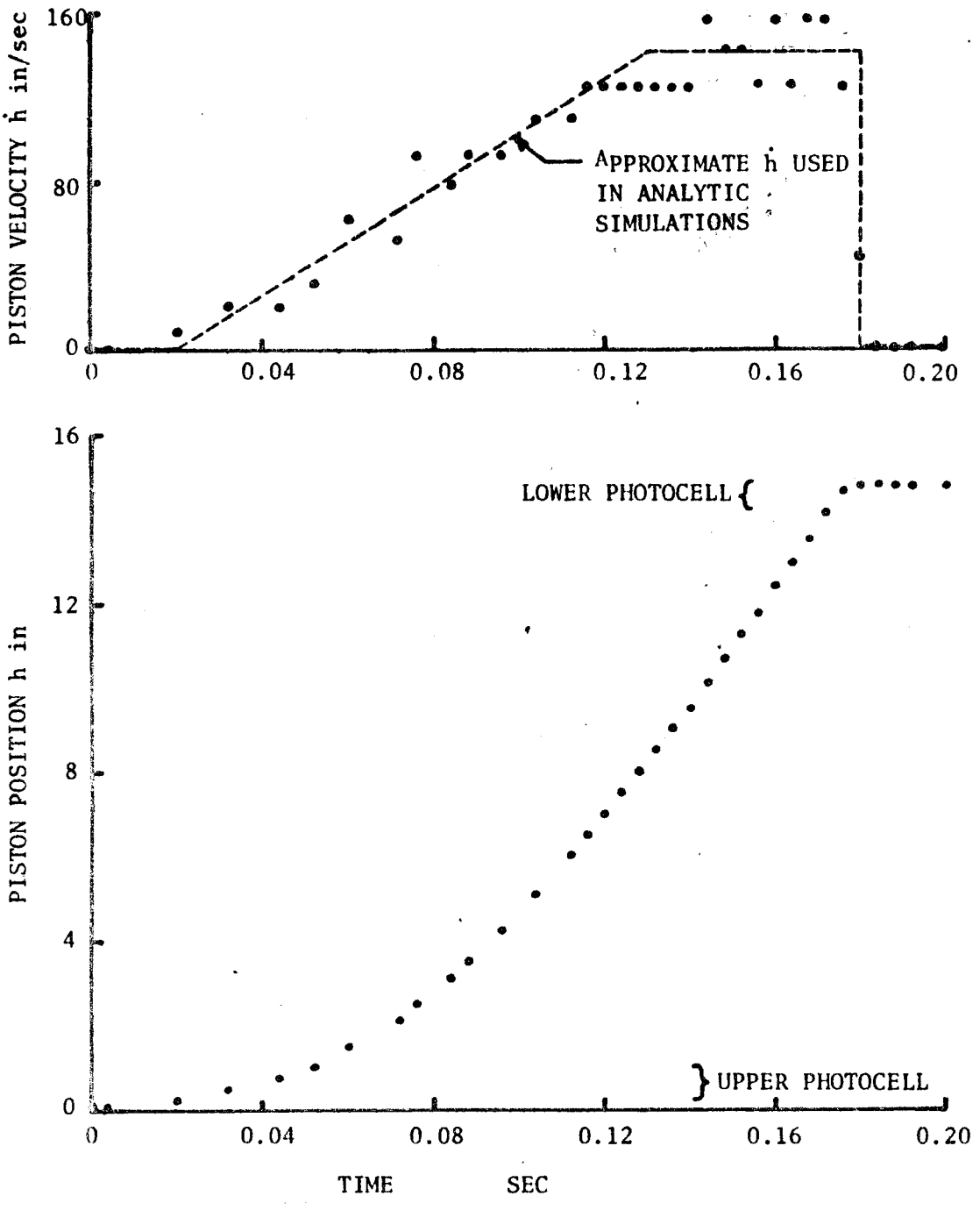

Figure 13 Typical Pivot Axis Time History for Motion Tests

TABLE I

Experimental Conditions and Results for the Wright-Patterson Vane

Run #	Tunnel q psf	Equivalent Airspeed mph	α_1/α_o no	α_2/α_1 no	T_1-T_o ms	T_2-T_1 ms	ζ_{eff} no		f_n Hz		Piston Travel Duration ms	Angle at Impact deg
1	0.535	14.5	0.10		520		0.59		1.19			
2	0.535	14.5	0.15		517		0.52		1.13			
3	1.144	21.2	0.33	0.12	380	380	0.33	0.56	1.39	1.32		
4	2.324	30.2	0.55	0.30	295	330	0.19	0.36	1.73	1.62		
5	4.086	40.0	0.49	0.41	240	250	0.22	0.27	2.13	2.08		
6	6.388	50.0	0.55	0.35	205	185	0.19	0.32	2.48	2.85		
7	6.388	50.0	0.60	0.38	200	180	0.16	0.29	2.53	2.90		
8	9.195	60.0	0.47	0.43	160	160	0.23	0.26	3.21	3.24		
9	14.372	75.0	0.47	0.51	128	140	0.23	0.21	4.01	3.65		
10	14.372	75.0	0.50	0.46	140	130	0.22	0.24	3.66	3.96		
11	25.553	100.0	0.58	0.45	95	95	0.17	0.25	5.34	5.44		
12	25.553	100.0	0.50	0.48	105	100	0.22	0.23	4.88	5.14		
13	39.926	125.0	0.55	0.42	85	75	0.19	0.27	5.99	6.92		
14	39.926	125.0	0.56	0.43	85	80	0.18	0.26	5.98	6.47		
15	57.495	150.0	0.51	0.49	65	65	0.21	0.22	7.87	7.88		
16	78.261	175.0	0.43	0.42	56	54	0.26	0.27	9.24	9.61		
17	78.261	175.0	0.55	0.38	56	54	0.19	0.29	9.09	9.67		
18	0.515	14.2	0.50	0.40	390	500	0.22	0.28	1.31	1.04	130	8.1
19	1.003	19.8	0.50	0.60	275	350	0.22	0.16	1.86	1.45	137	9.0
20	1.040	20.2	0.58	0.45	270	300	0.17	0.25	1.88	1.72	138	6.9
21	2.391	30.6	0.59	0.55	180	220	0.16	0.19	2.81	2.31	141	5.6
22	4.086	40.0	0.61	0.38	160	190	0.16	0.29	3.16	2.75	108	6.8
23	4.086	40.0	0.54	0.43	170	190	0.19	0.26	2.99	2.72	100	5.6
24	9.195	60.0	0.50	0.70	120	160	0.22	0.11	4.27	3.14	100	7.2
25	25.553	100.0	0.46	0.43	95	95	0.24	0.26	5.42	5.45	132	3.8
26	57.495	150.0	0.62	0.38	75	65	0.15	0.29	6.74	8.04	138	2.5

Note: All tests were conducted at $P_{amb} \approx 29.2$ in Hg and $T_{amb} \approx 75°$. The base motion ζ's and f_n's were based on motions subsequent to the impact effects.

and α_n denotes the amplitude of the nth extrema.

The natural frequency was then determined from the damped period. Since the interval between extrema is half the damped period,

we have $$T_{n+1} - T_n = \frac{1}{2f_n\sqrt{1-\zeta^2}} \tag{25}$$

or $$f_n = \frac{1}{2\ (T_{n+1}-T_n)\ \sqrt{1-\zeta^2}} \tag{26}$$

where T_n denotes the time of occurance of the nth extrema.

Comparison of Theory with Experiment

Wright-Patterson Vane

The Wright-Patterson vane is a rectangle of aspect ratio A = 0.5 which is pivoted about its leading edge. From Table I of Gersten [7] we can obtain the center of pressure location, as a fraction of chord, by dividing $C_{L\alpha}$ by $C_{M\alpha}$. The results are plotted in Figure 14. Unfortunately, one must extrapolate for aspect ratios less than one. Gersten's incompressible approach would extrapolate to an center of pressure at the leading edge for an aspect ratio equal to zero. Using an "eyeballed" fit to these points, the center of pressure is about 14 percent of the chord. One should note that ordinary and spline polynomial fitting schemes were attempted, but the resulting equations were obviously unrealistic because of inappropriate extrema. Slender body theory predicts a lift coefficien $C_{L\alpha} = \pi A/2 = \pi(0.5)/2 = 0.785$. The natural frequency prediction is then, from equation (12),

$$\omega_n = \sqrt{\frac{C_{L\alpha}\, \ell S q}{J'}} = \sqrt{\frac{(0.785)[0.14(4.76)][(4.75)(2.375)]}{0.0012}}\sqrt{q} = 70.05\sqrt{q}$$

where the aero inertia term was neglected and q is measured in psi. Performing some conversions, one has

$$f_n = \frac{70.05}{2\pi}\sqrt{\frac{q}{144}} = 0.929\sqrt{q}$$

where the dynamic pressure q is now measured in psf. This prediction is compared with the wind tunnel results in Figure 15 where the equivalent airspeed $U_{eqv} = \sqrt{2q/\rho_o}$ and $\rho_o = 1.08 \cdot .10^{-7}$ $lb_f\text{-}sec^2/in^4$. The aerodynamic damping predicted by equation (14)

$$\zeta = \frac{(2\ell+b)(\ell+b)}{4\ell}\sqrt{\frac{C_{L\alpha}\, \ell\, \rho_o\, S}{2J'}} = \frac{[2(0.665) + 2.375][0.665 + 2.375]}{4(0.665)}$$

$$\cdot\sqrt{\frac{(0.785)(0.665)(1.08 \cdot 10^{-7})(11.28)}{2(0.0012)}}$$

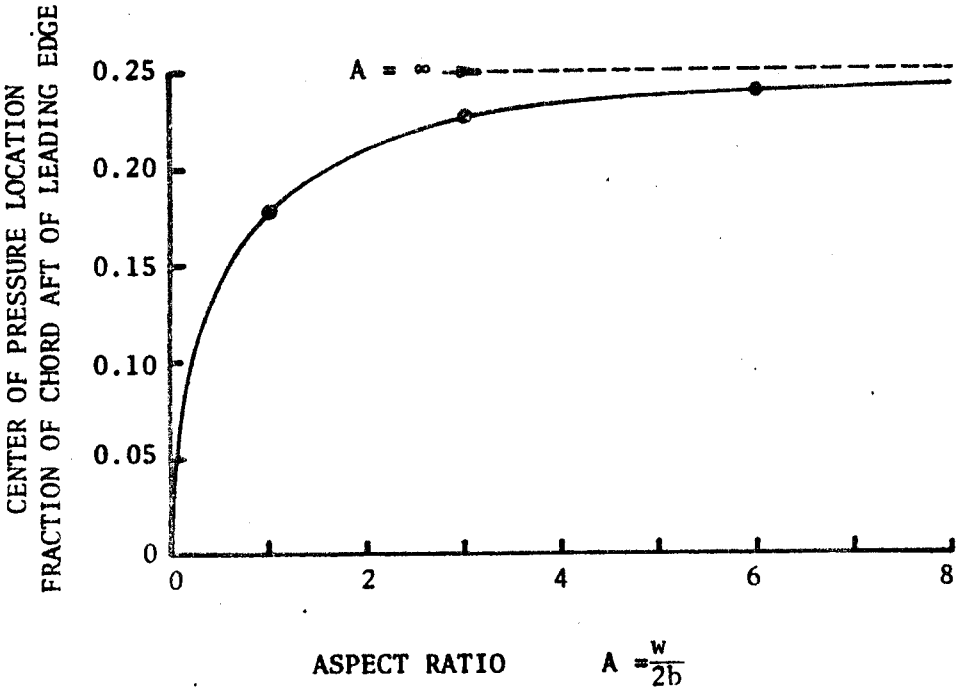

Figure 14 Center of Pressure Location versus Aspect Ratio for Rectangular Wings (Points due to Gersten [7])

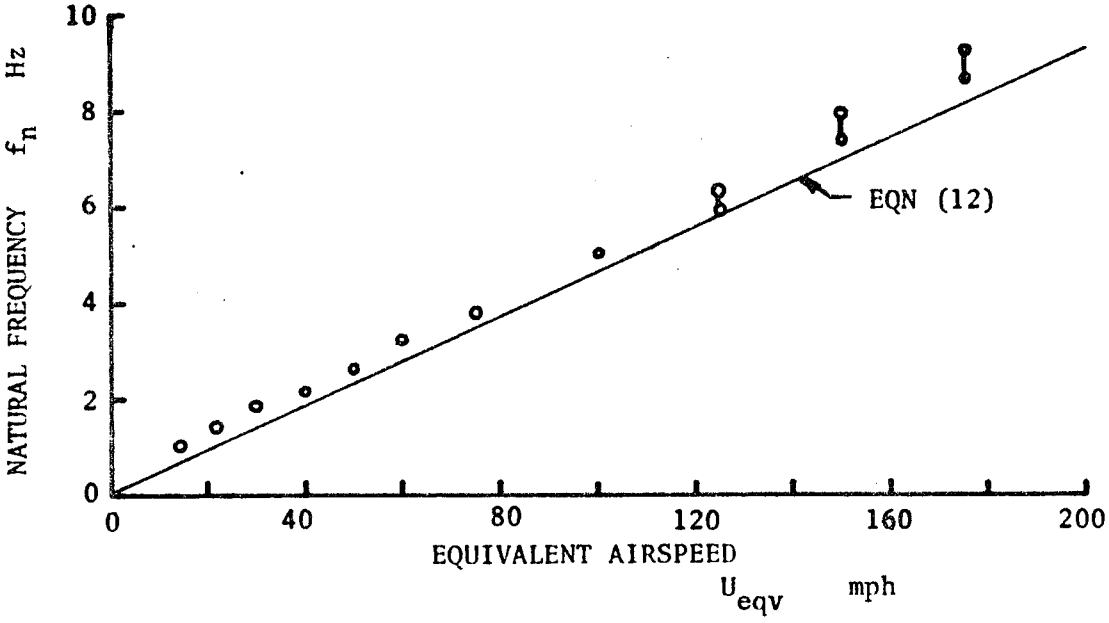

Figure 15 Comparison of Natural Frequency Prediction and Experiment for the Wright-Patterson Vane (Release from an Initial Angle Tests; Table I, Runs 1-17)

$$\zeta = 4.23\ (0.016) = 0.069$$

is compared with experiment in Figure 16. Note that this theoretical damping is independent of equivalent airspeed. For relatively large airspeeds (U_{eqv} > 50 mph), the observed damping is also essentially constant although the observed value is 2 to 3 times that predicted by equation (14). The damping predicted by a published formula is much smaller, i.e., equation (18), the limiting case of equation (14) for $\ell >> b$,

$$\zeta_{limit} = \frac{\ell}{2}\frac{\omega_n}{U} = \frac{0.665}{2}\ (0.016) = 0.0053$$

The increased damping noted at low airspeeds for this vane was attributed to mechanical friction. As noted in the theory section, two types of friction were considered: viscous and dry. Viscous friction is the type most commonly considered in theoretical developments [2,4,5] -- primarily because of the analytic convenience of linearity. A computer program was written which solves equation (11) by means of a 4th-order variable step, Runge-Kutta, numerical differential equation solver. A listing is included as Appendix A. A linear interpolator is used to approximate any arbitrary variation in the velocity of the pivot axis. Figure 17 shows fitted theoretical solutions to the lowest airspeed runs. By trial and error, both a viscous and a dry friction solution can be made to reasonably approximate the experimental data for this (for that matter, any) single run. However, it is felt that the dry friction solution is more appropriate for several reasons. The main justification is simply due to the physical construction of the vane assembly. Possible friction sources are almost all the result of the relative sliding of mechanical surfaces, i.e., dry friction. This is typical, in fact, of

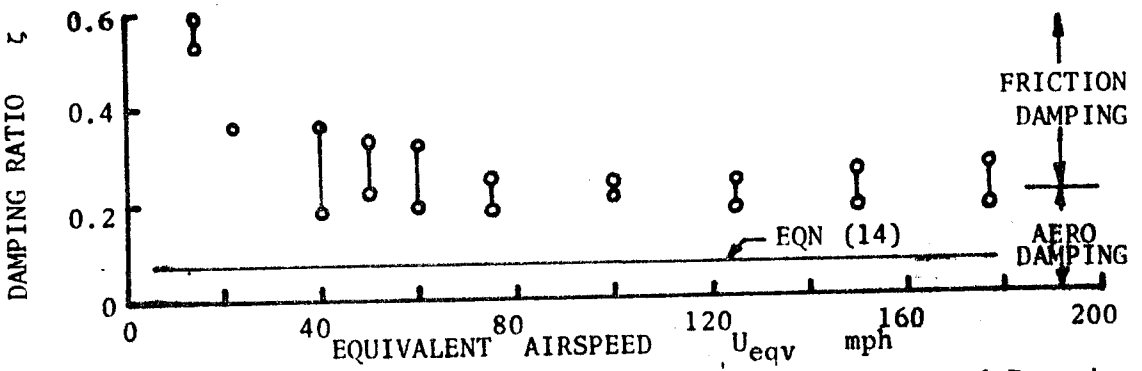

Figure 16 Comparison of Damping Ratio Prediction and Experiment For the Wright-Patterson Vane (Release from an Initial Angle Tests; Table I, Runs 1-17)

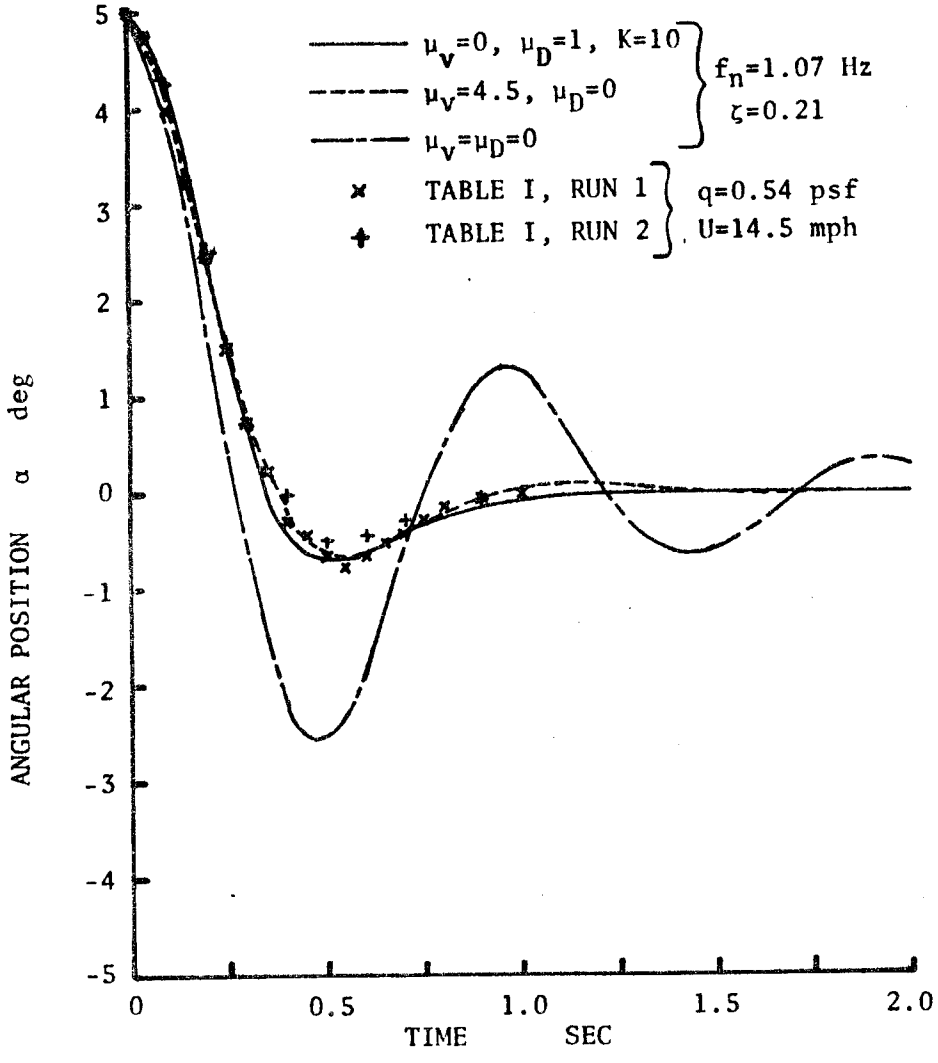

Figure 17 Comparison of Various Fitted Models with Experiment for Low-Speed Tests of the Wright-Patterson Vane

most vanes except for those where a discrete viscous damper was intentionally added to the pivot shaft [5,8]. Secondly, at very small angles of attack, the vane damping effectively increases -- again a characteristic of dry friction only. For example, Figure 18 compares the response for various initial angles of attack for only dry and only viscous friction. Obviously, only the dry friction can provide the amplitude dependent behavior observed. Thirdly, the dry friction's effects diminish more rapidly with airspeed then does the viscous friction. Figures 19 and 20 show the response for medium and relatively high speed tests of the Wright-Patterson vane. Again, the dry friction more closely approximates the experimental behavior. Finally, dry friction is commonly reduced by small mechanical motions -- often called dithering when done intentionally. In the pivot axis motion tests, even at the lowest airspeeds, significant frictional effects were not observed -- only the typical aerodynamic damping. Figure 21 shows a low speed response.

Figures 22, 23, and 24 compares the predictions of the theoretical model with the experimental pivot axis motion results. Despite some increased scatter, reasonable agreement is again noted. The natural frequency and damping ratio data was obtained after the vane reversal effects at impact had subsided, and the basic second order system response returned (see Figure 11). The angle at impact was taken to be representative of the true behavior of the vane due to motions of its pivot axis. The subsequent rapid reversal of the vane was speculated to be the result of the vane's bearings instantaneously locking up under the large impact loads.

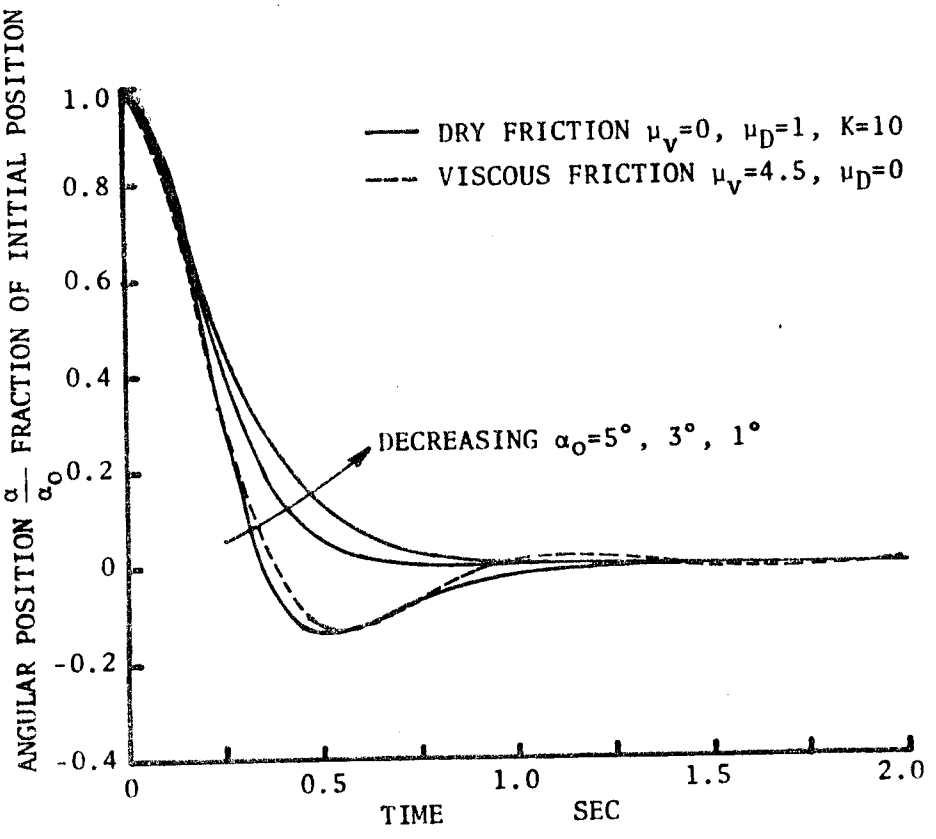

Figure 18 Typical Amplitude Dependent Effects of Dry versus Viscous Friction (f_n=1.07, ζ=0.21)

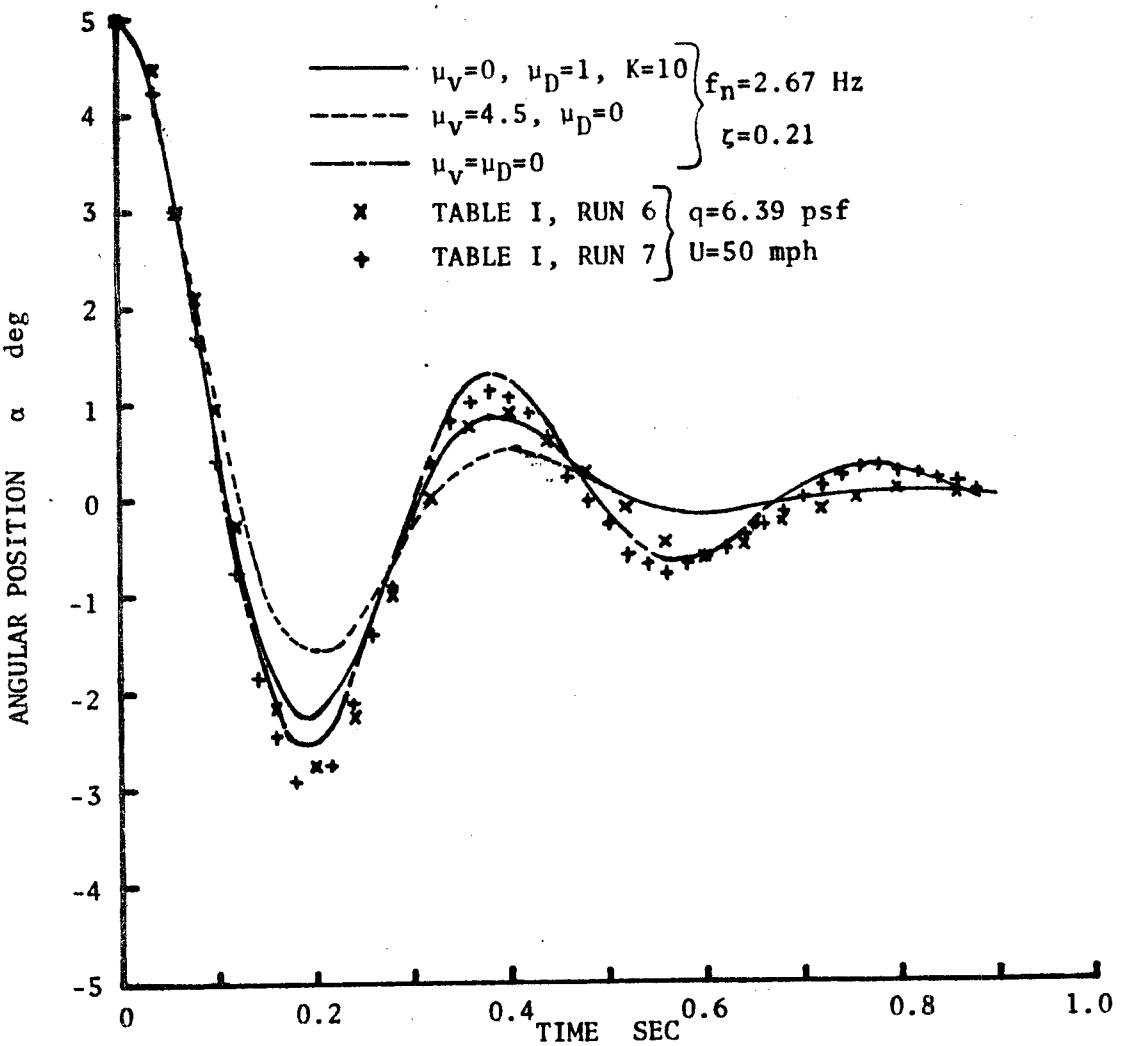

Figure 19 Comparison of Various Fitted Models with Experiment for Mid-Speed Tests of the Wright-Patterson Vane

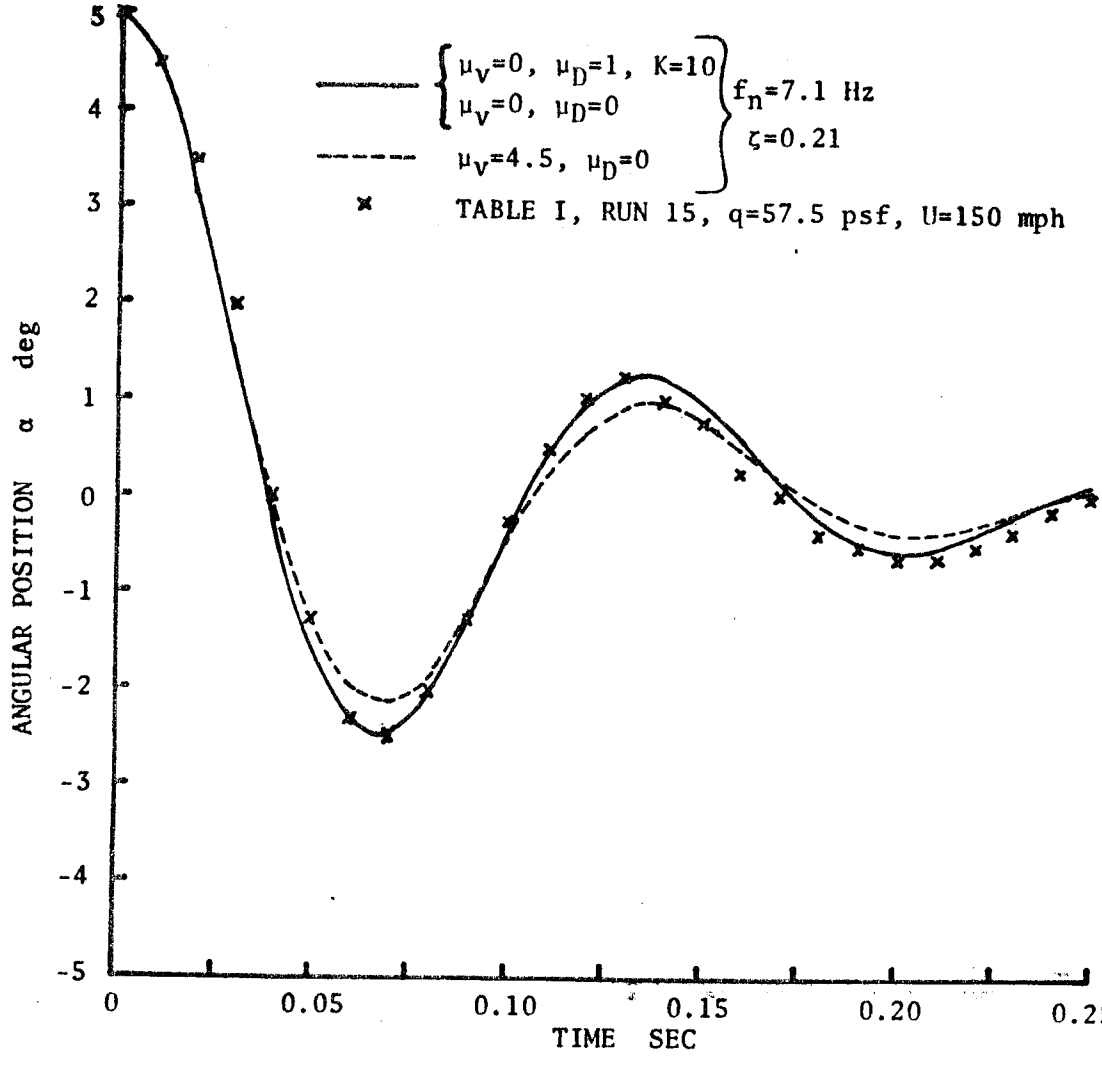

Figure 20 Comparison of Various Fitted Models with Experiment for a High Speed Test of the Wright-Patterson Vane

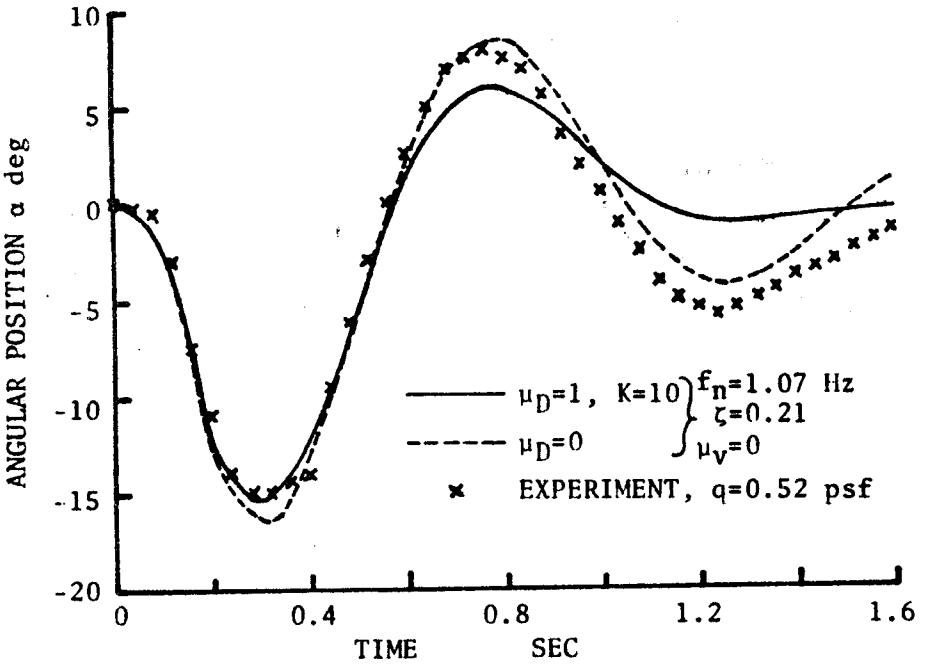

Figure 21 Comparison of Various Fitted Models with Experiment for a Pivot Axis Motion Test of the Wright-Patterson Vane

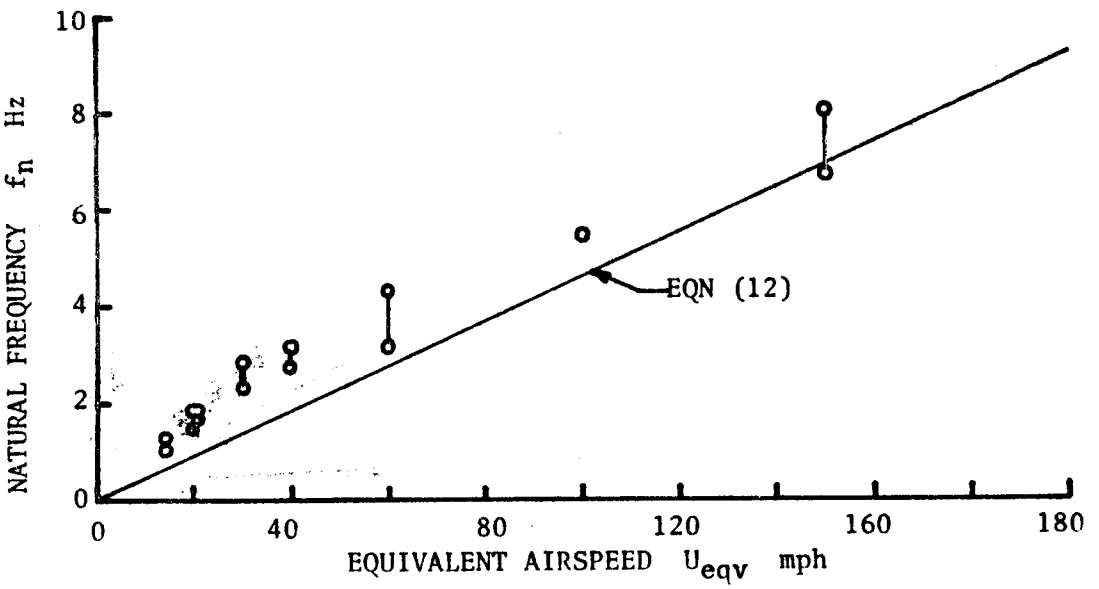

Figure 22 Comparison of Natural Frequency Prediction and Experiment for the Wright-Patterson Vane (Pivot Axis Motion Tests; Table I, Runs 8-26)

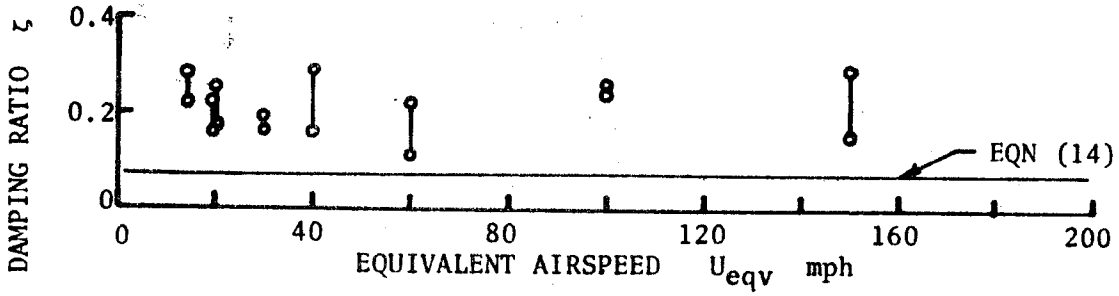

Figure 23 Comparison of Damping Ratio Prediction and Experiment for the Wright-Patterson Vane (Pivot Axis Motion Tests; Table I, Runs 18-26)

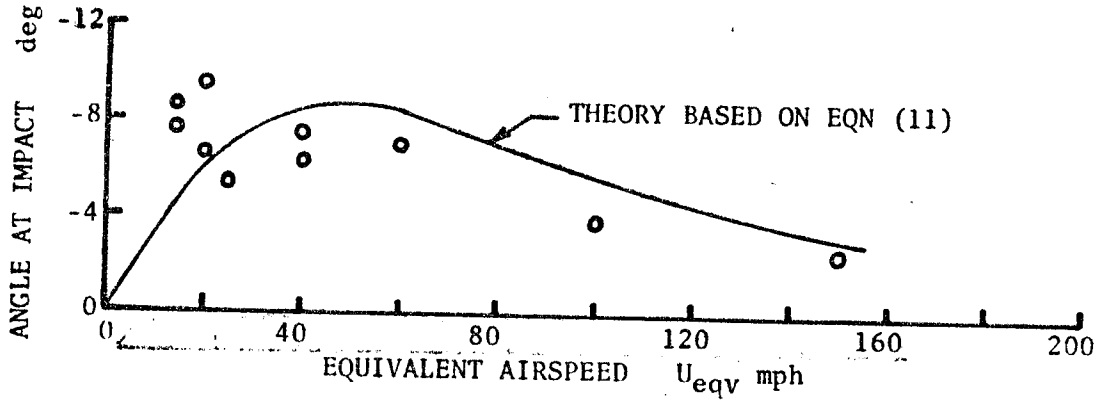

Figure 24 Angular Position at Impact (T=0.16 sec) Prediction versus Experiment for Pivot Axis Motion Tests of the Wright-Patterson Vane (Table I, Runs 18-26; $\bar{h}$ as in Figure 13)

As a qualitative justification of this assumed bearing lock-up phenomena, the potential aerodynamic moment of a uniformly loaded, cantilevered vane was investigated. This possibility was selected for two reasons. First, cracks were noted in the vane's paint just aft of its attachment to the pivot shaft. Secondly, an aerodynamic phenomena was suspected because the amplitude of the reversal varied with airspeed (see Figure 25).

First, consider a constant thickness, rectangular section, cantilever beam. While the vane is anything but slender, slender beam theory can be used to provide a 20% type prediction which is sufficient for our purpose. Figure 26 indicates the coordinate system used. Most any mechanics of materials text has the required solution for the deflection, z, of a uniform beam of length L assuming a constant modulus of elasticity E and section area moment of inertia I. Since the density and modulus of elasticity of fiberglass is much greater than balsa, the effects of the balsa sheeting were neglected, and the vane was treated as if it were just the fiberglass sheet. The deflection of such a beam subjected to a uniform load of W pounds per inch is found to be

$$z = -\frac{W}{24EI}\left[(L-x)^4 - 4L^3\,(L-x) + 3L^4\right] \tag{27}$$

If we consider the effective angle of attack α_o due to just the static deflection,

$$\alpha_o \approx \frac{z_{max}}{L} = \frac{WL^3}{8EI} \quad \text{where} \quad I = \frac{wt^3}{12} \tag{28}$$

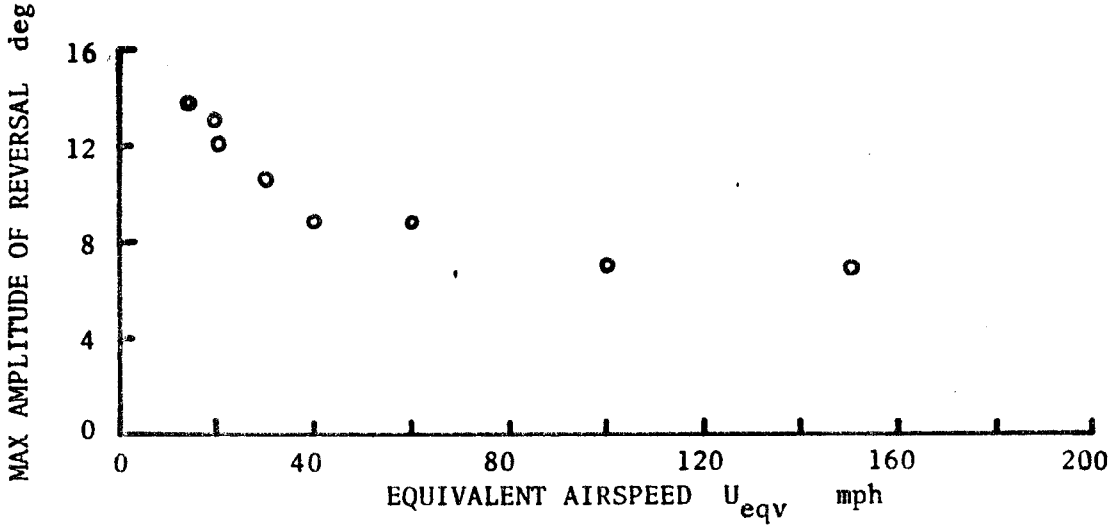

Figure 25 Maximum Van Reversal Subsequent to Impact versus Airspeed

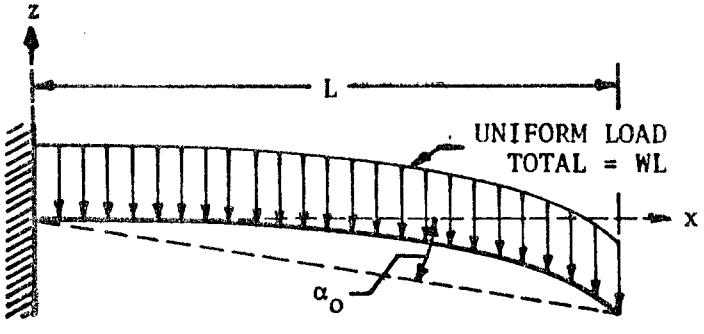

Figure 26 Uniformly Loaded Cantilever Beam

If we further consider the additional aerodynamic forces due to the deformed beam's camber, we obtain

$$C_{m_{L.E.}} = -\frac{\pi}{2}\left(\alpha_o + \frac{17WL^3}{96EI}\right) \simeq -\frac{\pi}{2}(2.5\,\alpha_o) = -\frac{1}{4}C_{\ell\alpha}\frac{5WL^3}{16EI} \qquad (29)$$

by applying classical Fourier series, 2-dimensional airfoil analysis, e.g., see McCormick [11]. Note that camber has the effect of increasing the angle of attack by a factor of 2.5. A typical Young's modulus E for fiberglass is $2 \cdot 10^6$ psi. Fiberglass has a weight density of about 0.06 lb_f/in^3. The inertial acceleration at impact is approximately (from Figure 13).

$$\frac{\Delta\dot{h}}{\Delta T} \simeq \frac{140.5 - 0}{0.004} = 35125 \text{ in/sec}^2 \simeq 91 \text{ g's}$$

The effective angle of attack is then

$$\alpha_{eff} = \frac{5[\rho wt\,\frac{\Delta\dot{h}}{\Delta T}]L^3}{16E[wt^3/12]} = \frac{15}{4}\frac{L^3}{E}\frac{\rho}{t^2}\frac{\Delta\dot{h}}{\Delta T} = \frac{15}{4}\frac{(4.375)^3}{(2\cdot 10^6)} = \frac{(0.06)}{(0.062)^2}(91) =$$

$$.223 \text{ rad} = 12.8 \text{ deg.}$$

This estimate is somewhat conservative in that the basic deflection solution, equation (27), assumes slowly applied loads, and an impulsive application could lead to twice as much deflection. When the bearings release, one then has a deformed flat plate vibrating in the free-free mode. It was beyond the scope of this study to investigate the damped oscillation of such a plate immersed in an airstream. Nevertheless, a high frequency oscillitory motion was indeed observed within the overall motion subsequent to impact. Most importantly, the estimated effective angle of deflection is sufficient to cause the magnitude of overall vane motions noted in the experiments subsequent to impact.

Langley Vane

Richardson [4] tested an all-balsa vane used by NASA Langley for gust measurements. This vane is geometrically identical to the Wright-Patterson vane, but it has a smaller inertia ($J = 0.00014$ in-lb$_f$-sec^2). Thus, the vane's dynamic characteristics are predicted to be

$$f_n = 2.72\sqrt{q} \quad \text{and} \quad \zeta = 0.20$$

Release from an initial angle tests were conducted at Mach number $M = 0.18$, 0.27, and 1.6. Table 2 summarizes Richardson's test results. Several comments are in order.

First, the natural frequency prediction again shows reasonable agreement (less than 20% error) as with the Wright-Patterson vane. Significantly, this prediction is valid for the supersonic case as well -- in spite of the theory's incompressible background. Recall that such a possibility could be inferred from slender body theory. Secondly, the damping ratio is only predicted within a factor of 2 to 3 -- again like the Wright-Patterson vane results. However, it is felt that much of the apparent damping of the Langley vane is due to mechanical friction. Because of the Langley vane's lower inertia, the frictional terms can remain significant for higher airspeeds. Further, the Langley vane uses a potentiometer as the sensor. The potentiometer's inherent wiper contact pressure could only lead to a relative increase in dry friction effects. The amplitude dependence of the effective damping (see Table 2) is further evidence that dry friction effects are significant in the Langley tests. Richardson notes that, for a given initial amplitude, the damping varies approximately as the square root of the air's density. This would imply that the velocity in equation 14 should be the actual

TABLE II

Experimental Conditions and Results for Langley Vane (after Richardson [4])

M no.	Tunnel q psf	Air Density ρ $lb_f\text{-}sec^2/in^4$	Initial Angle of Attack α_o deg	α_1/α_o no.	T_1-T_o ms	Experimental f_n Hz	Experimental ζ no.	Predicted f_n Hz	Predicted ζ no.
0.183	50	$1.08 \cdot 10^{-7}$	3.6	0.07	28	23.5	0.65	19.2	0.20
0.183	50	$1.08 \cdot 10^{-7}$	2.8	0.06	31	21.7	0.67	19.2	0.20
0.183	50	$1.08 \cdot 10^{-7}$	2.0		17*		>.7	19.2	0.20
0.183	50	$1.08 \cdot 10^{-7}$	1.0		14*		>.7	19.2	0.20
0.268	50	$5.08 \cdot 10^{-8}$	3.5	0.20	25	22.4	0.45	19.2	0.20
0.268	50	$5.08 \cdot 10^{-8}$	2.6	0.15	26	22.5	0.52	19.2	0.20
0.268	50	$5.08 \cdot 10^{-8}$	1.7	0.11	25	24.3	0.57	19.2	0.20
0.268	50	$5.08 \cdot 10^{-8}$	0.8	0.06	24	28.0	0.67	19.2	0.20
1.6	190	$7.88 \cdot 10^{-9}$	2.3	0.45	13	39.7	0.25	37.5	0.20
1.6	190	$7.88 \cdot 10^{-9}$	1.4	0.26	14	38.8	0.39	37.5	0.20
1.6	190	$7.88 \cdot 10^{-9}$	0.9	0.08	15	42.9	0.63	37.5	0.20

*rise time from 10% to 90% amplitude

rather than the equivalent airspeed. It is the present author's opinion that equivalent airspeed is more consistent with the theoretical development and other results to be subsequently discussed. The apparent decrease in dry friction damping could very well result from the increased mechanical dithering provided by the higher speed airstream. Further tests are needed to completely resolve the issue. Finally, it should be noted that Richardson performed some special tests to determine the center of pressure of the Langley vane. The c.p. was found to be 8.8% of the chord aft of the pivot axis which was located at the 2.5% chord station. However, the inferred lift coefficient $C_{L\alpha}$ = 1.52 is almost double that predicted by well established theoretical methods. Nevertheless, the theoretical methods recommended in this report for rectangular vanes (Equation 20 and Figure 14) predict a $C_{L\alpha}\ell$ product which is not inconsistent with Richardson's test results.

Edwards Vane

Another vane configuration is the dual triangle arrangement used by the AF Flight Test Center at Edwards AFB, California. This vane is used in conjunction with flight path accelerometers for dynamic aircraft performance testing. Olsen [1] reported the results of release from an initial angle tests conducted at Mach numbers M = 0.3, 0.5, 0.7, 1.5, 2.5, and 3. The significant dimensions of this vane are shown in Figure 27. Slender body theory predicts a center of pressure located at the centroid of the "effective" planform area. Any wing area downstream of the widest span dimension is considered ineffective. All of this planform's area is "effective," and the area centroid is located 3.95 inch aft of the apex. Thus, the center of pressure is 2.40 inches aft

of the pivot axis. Again, according to slender body theory, the vane lift coefficient is

$$C_{L\alpha} = \pi A/2 = \pi(0.714)/2 = 1.12$$

The vane's predicted natural frequency is then, from equation 12,

$$f_n = \frac{1}{2\pi}\sqrt{\frac{C_{L\alpha}\ell\ S\ q}{J'}} = \frac{1}{2\pi}\sqrt{\frac{(1.12)(2.40)[2(8.75)]}{0.011}\left[\frac{q}{144}\right]} = 0.867\sqrt{q}$$

where q is again the dynamic pressure in psf. This prediction is compared with Olsen's experimental results in Figure 28. Again, the prediction is within 10% except for the two lower supersonic tests where the error is about 20%. The limiting value of damping is predicted from equation (18) as

$$\zeta_{limit} = \frac{\ell}{2}\frac{\omega_n}{U} = \frac{\ell}{2}\sqrt{\frac{C_{L\alpha}\ell\ \rho_o\ S}{2J'}} = \frac{2.40}{2}\sqrt{\frac{(1.12)(2.40)(1.08\cdot10^{-7})[2(8.75)]}{2(0.011)}}$$

$$= 1.20(0.0152) = 0.018$$

However, to evaluate equation (14), one needs to define the semichord b for a non-rectangular planform. With little justification, let's use an average semichord

$$b_{avg} = \frac{S}{2w} = \frac{8.75}{2(2.5)} = 1.75 \text{ in}$$

Then, the damping predicted by equation (14) is

$$\zeta = \frac{(2\ell+b)(\ell+b)}{4\ell}\frac{\omega_n}{U} = \frac{[2(2.40)+1.75][2.40+1.75]}{4(2.40)}(0.0152) = 2.83(0.0152) = 0.043$$

The experimental data ranges in the vicinity of these predictions. Again, the prediction of equation (14) matches the data within a factor of 2 or so. Figures 28, 29 and Table 3 summarize Olsen's results. Note that, for this vane, the damping ratio does not show any obvious dependence on the square root of the density.

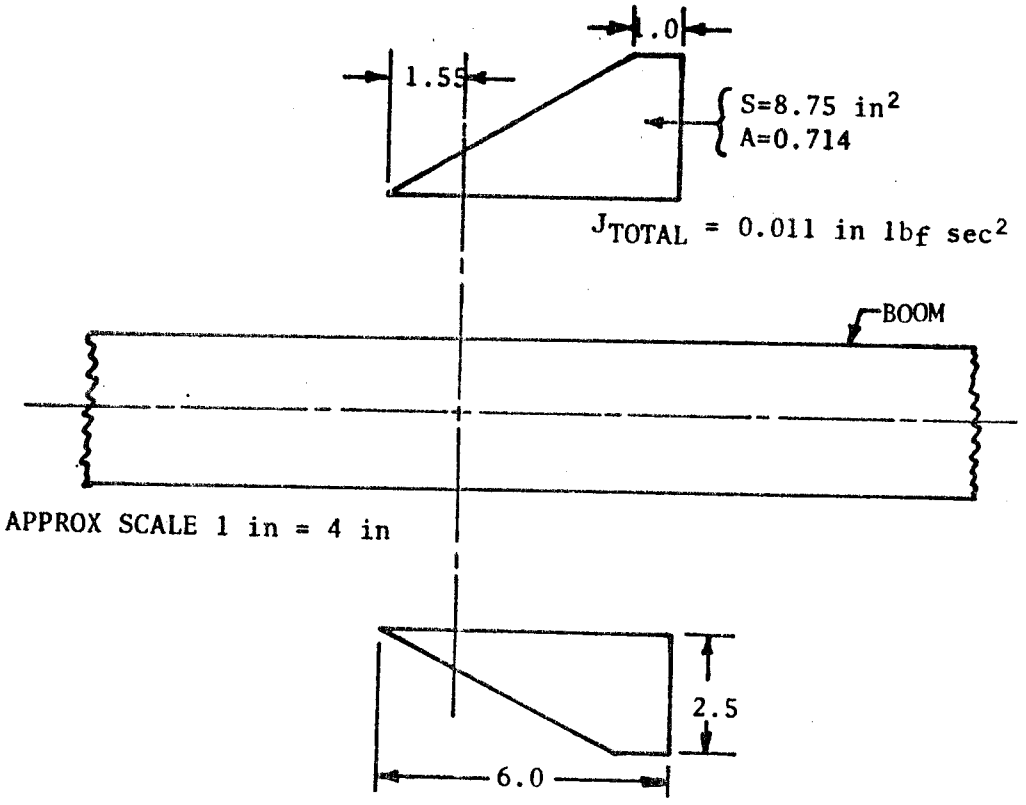

Figure 27 Geometry of Edwards Vane Assembly

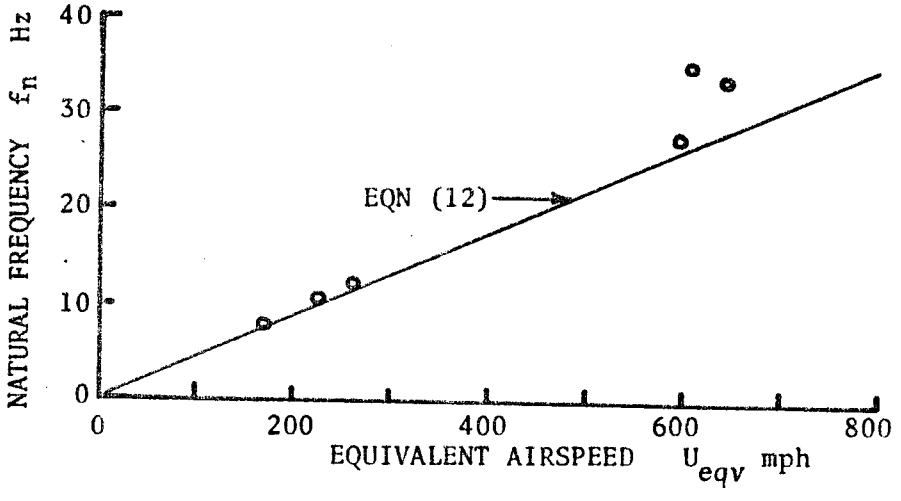

Figure 28 Comparison of Natural Frequency Prediction and Experiment for the Edwards Vane (Table III; data due to Olsen [1])

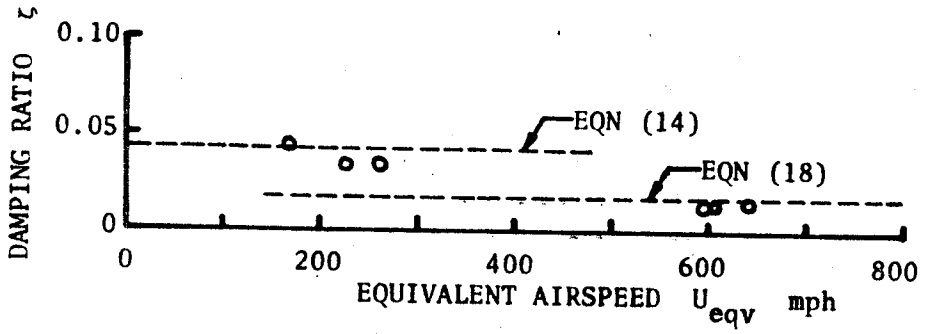

Figure 29 Comparison of Damping Ratio Prediction and Experiment for the Edwards vane (Table III; data due to Olsen [1])

TABLE III

Experimental Conditions and Results for the Edwards Vane (after Olsen [1])

Mach No. M no.	Tunnel q psf	U_{eqv} mph	$\sqrt{\rho/\rho_o}$ no.	Experimental f_n Hz	Experimental ζ no.	Predicted f_n Hz	Predicted ζ no.
0.31	72.2	168	0.69	7.8	0.045	7.4	0.043
0.51	130.6	226	0.57	10.5	0.034	9.9	0.043
0.71	172.8	260	0.49	12.1	0.034	11.4	0.043
1.5	935.7	605	0.61	35.0	0.015	26.5	0.043
2.5	1047.1	640	0.48	33.4	0.016	28.0	0.043
3.0	905.0	595	0.42	27.2	0.013	26.1	0.043

NCAR Vane

Lenschow [5] reports on some wind tunnel tests performed on a rectangular vane which is pivoted about its leading edge. Constructed of cast polyester fiberglass, the vane has a chord of 2.5 inches and a width of 1 inch. The moment of inertia of the assembly is about $1.8 \cdot 10^{-5}$ in lb_f sec^2. A lift coefficient of 1.3 was apparently inferred from a static torque measurement and an assumed center of pressure at the quarter chord. Slender body theory predicts

$$C_{L\alpha} = \pi A/2 = \pi \frac{(1)^2}{(1)(2.5)} /2 = 0.628$$

This latter value of $C_{L\alpha}$ and the experimental $C_{M\alpha}$ would imply a center of pressure at about mid-chord. Lenschow also noted that the experimental damping was about double that predicted by the theory. The message here is again that the prediction of $C_{M\alpha} = C_{L\alpha}\ell$ for low aspect ratio planforms is difficult at best, but that, given a reasonable value for $C_{M\alpha}$, the predictions of equation (11) will be reasonable.

Design Considerations

The question of a user would be how does one design a vane for a given set of desired characteristics. For some guidance, let's first consider a rectangular vane and ignore the effects of the counterweight. Then equations (12) and (14) become

$$\omega_n \simeq \sqrt{\frac{C_{L\alpha}\, \ell\, q\, S}{\rho_{vane}\, St(\ell^2+\ell b+b^2)}} \quad \text{and} \quad \zeta \simeq \frac{(2\ell^2+3\ell b+b^2)}{4\ell}\sqrt{\frac{C_{L\alpha}\, \ell\, \rho_{air}\, S}{2\rho_{vane}\, St(\ell^2+\ell b+b^2)}}$$

For a relatively long pivot arm ($\ell > > b$), these become

$$\omega_n \simeq \sqrt{\frac{C_{L\alpha}\, q}{\rho_{vane}\, t\ell}} \quad \text{and} \quad \zeta \simeq \sqrt{\frac{C_{L\alpha}\, \rho_{air}\, \ell}{8\rho_{vane}}} \quad \text{for } \ell > > b \tag{30}$$

In this case, the desire for a large ω_n and reasonably large damping ($\zeta \simeq 0.7$ is typically desired) are contradictory, since a large ω_n would imply a small ℓ and vice versa. On the other hand, for $\ell << b$, these become

$$\omega_n \simeq \sqrt{\frac{C_{L\alpha}\, q\, \ell}{\rho_{vane}\, t\, b^2}} \quad \text{and} \quad \zeta \simeq \sqrt{\frac{C_{L\alpha}\, \rho_{air}\, b^2}{32\, \rho_{vane}\, t\ell}} \quad \text{for } \ell << b \tag{31}$$

Again, the influence of ℓ on the two terms is contradictory, but it is just the opposite of the other limiting case. Thus, we can decrease ω_n by both decreasing and increasing ℓ. A maximum must exist for ω_n's variation with ℓ, i.e., when $\frac{\partial \omega_n}{\partial \ell} = 0$. With the other parameters held constant, ω_n then has a maximum when $\ell = b$. This particular value is of little direct use because of the many approximations inherent in its development. However, one may conclude that the common scheme of a leading edge pivot is near optimum from the standpoint of maximizing the natural frequency. One commonly then accepts the resulting damping.

For most designs in use, the damping is small -- on the order of 0.2 or less. The most obvious way to both increase the natural frequency and the damping is to reduce the assembly's mass moment of inertia -- hence the common use of balsa and fiberglass construction. However, one must be careful because if the inertia becomes too small, the dry friction effects present in any mechanical device will remain dominant in the observed behavior (recall the Langley vane). A better alternative would be to intentionally add a viscous damper, e.g., see Telford and Warner [8] or one would enhance the viscous effects of the airstream, e.g., the perforated vane scheme of Lenschow [5]. Another alternative is to change to the constrained vane scheme of Crooks [12]. Note that while equation (29) seems to imply that only the vane's density and thickness have an effect on natural frequency, the vane area S does still have an effect -- but through $C_{L\alpha}$. Recall that for a leading edge pivot, $\ell \approx b/2$, so that, for a fixed ℓ, an increased area implies an increased aspect ratio and thus $C_{L\alpha}$.

Consider now the counterweight design. Since it is usually desired to have the total inertia to be as small as possible, one needs a very dense counterweight with as short a support shaft as is possible [see equations (5) and (9)].

Next, let's consider the conditions needed for the simple model, equation (17), to be valid. First, the aerodynamic inertia term will be negligible if

$$J_{vane} >> J_{aero} \tag{31}$$

or, neglecting the counterweight's inertia, if

$$\rho_{vane}\, ST\, (\ell^2 + \ell b + \frac{7}{12} b^2) >> (\ell^2 + \ell b + \frac{1}{4} b^2)\, \frac{\pi}{2}\, \rho_{air}\, bS \tag{32}$$

or, approximately, if $\rho_{vane} >> \rho_{air} \frac{\pi b}{2t}$. (33)

For the acceleration of the pivot axis to be negligible, we need

$$\dot{h} >> \frac{2\ell + b}{4\ell} \frac{b}{U} \ddot{h} \tag{34}$$

For example, assuming a sinusoidal variation of the base such that $h(t) = h_o \sin \omega T$, then $\dot{h} = \omega h_o \cos \omega T$ and $\ddot{h} = -\omega^2 \sin \omega T$. Considering magnitudes only, we need

$$\omega h_o >> \frac{2\ell+b}{4\ell} \frac{b}{U} \omega^2 h_o \quad \text{or} \quad \frac{2\ell+b}{4\ell} \frac{b}{U} \omega << 1 \tag{35}$$

For reasonable airspeeds, this would be valid for all but the highest frequencies or, equivalently, impulsive like motions. For that matter, the influence of the pivot axis velocity may often be negligible. The effect of the motion is to produce an extraneous effective angle of attack whose magnitude is given by

$$\alpha_o = \frac{\dot{h}}{U} = \frac{\omega h_o}{U} \tag{36}$$

for low frequency, sinusoidal axis motions. For example, the Wright-Patterson vane is mounted on an instrumentation boom whose natural frequency is about 14 Hz. Vibration amplitudes on the order of 2 inches have been observed in flight. For a typical thunderstorm penetration speed of 300 mph = 5280 in/sec, this boom motion could generate an error whose amplitude is on the order of

$$\alpha_o = \frac{[2\pi(14)][2]}{5280} = 0.033 \text{ radian} = 1.9 \text{ degrees}$$

The significance of this term will depend on the intended use of the data. However, this example brings up a further point. The vane's natural frequency at 300 mph is also about 14 cps, so the error would dynamically increased for this lightly damped vane. To minimize these

effects, one must avoid using a vane at airspeeds where the vane's natural frequency is equal to or greater than that of its supporting boom. More precisely, assuming a sinusoidal input of the $h(T) = h_o e^{j\omega T}$ and a response of the form $\alpha = \alpha_o e^{j(\omega T+\phi)}$, we can obtain from equation (17) that

$$\alpha_o = \frac{\omega h_o/U}{\left[1-\left(\frac{\omega}{\omega_n}\right)^2\right]^2 + 2\zeta\frac{\omega}{\omega_n}^2} \quad \text{and} \quad \phi = \tan^{-1}\frac{1-\left(\frac{\omega}{\omega_n}\right)^2}{2\zeta(\omega/\omega_n)} \tag{37}$$

The magnitude α_o has a maximum when $\omega = \omega_n$. This maximum is then

$$\alpha_{o_{max}} = \frac{\omega_n h_o}{2\zeta U} \quad \text{or} \quad \left.\frac{\alpha_{o_{max}}}{\alpha_{o_{nominal}}}\right|_{\omega=\omega_n} = \frac{1}{2\zeta} \tag{38}$$

Equation (38) quantifies the dynamic magnifications possible, and why one wants to avoid low damping. If the boom's frequency is much greater than the natural frequency of the vane, the vane's dynamic behavior filters out the effects of these base motions (see equation (37) for $\omega >> \omega_n$). Thus, one needs a stiff instrumentation boom. Since this is often impossible because of weight limitations, one could conceptually electronically filter the contribution of the boom motion. Unfortunately, data frequencies in that same range would likewise be eliminated. Perhaps the best alternative would be to mount an accelerometer or some such device which could sense the magnitude of the pivot axis displacement with respect to its rigid body aircraft position. With this information and the model of equation (17), one may electronically cancel just the contributions of the boom motion.

Conclusions and Recommendations

1. A simple model of the dynamic behavior of an angle-of-attack vane assembly has been developed and experimentally verified by wind tunnel tests of three vane designs. The model is valid for all airspeeds (except possibly transonic). The natural frequency is predicted within $\pm$ 20%. Most of this error results from estimating the lift curve slope and center of pressure for the very small aspect ratio planforms in use. This error could be reduced to less than 10% if the actual $C_{L\alpha}\ell$ product of the vane were known. Note that a single low subsonic value is sufficient to predict behavior at all airspeeds. The damping ratio is only predicted within a factor of 2 to 3.

2. At the airspeeds in common use, extraneous angular motions introduced by typical transverse motions of the vane's pivot point may not be negligible.

3. The free stream velocity used with the model should be equivalent, rather than actual, airspeed.

4. Mechanical friction effects should be negligible for vanes in use at reasonable airspeeds except for very small angular deflections.

5. If the predicted aerodynamic damping is less than desired, viscous damping can be enhanced, e.g., by perforating the vane, or an alternate measurement scheme should be considered, e.g., the constrained vane discussed by Lenschow [5].

References

1. Olsen, W.M., "An Interim Report on Dynamic Performance Flight Testing," unpublished report, June 1973, Air Force Flight Test Center, Edwards AFB, Calif.

2. Pinsker, W.J.G., "The Static and Dynamic Response Properties of Incidence Vanes with Aerodynamic and Internal Viscous Damping," Aeronautical Research Council C.P. No. 652, August 1962, Ministry of Aviation, London.

3. Dunlap, E.W., and Porter, M.B., "Theory of the Measurement and Standardization of In-Flight Performance of Aircraft," FTC-TD-71-1, April 1971, Air Force Flight Test Center, Edwards AFB, Calif., pp. V-53 to V-55.

4. Richardson, N.R., "Dynamic and Static Wind Tunnel Tests of a Flow-Direction Vane," NASA TN D-6193, April 1971, Langley Research Center, Hampton, Virginia.

5. Lenschow, D.H., "Vanes for Sensing Incidence Angles of the Air from an Aircraft," Journal of Applied Meteorology, Vol. 10, No. 6, December 1971, pp. 1339-1343.

6. Bisplinghoff, R.L., Ashley, H., and Halfman, R.L., Aeroelasticity, Addison-Wesley, Reading, Mass., 1955, pp. 262-279.

7. Gersten, K., "Nonlinear Airfoil Theory for Rectangular Wings in Incompressible Flow," NASA RE 3-2-59W, February 1959, NASA, Washington, D.C.

8. Telford, J.W., and Warner, J., "On the Measurement from an Aircraft of Buoyancy and Vertical Air Velocity in Clouds," Journal of the Atmospheric Sciences, Vol. 19, 1962, pp. 415-423.

9. Jones, R.T., "Properties of Low-Aspect Ratio Pointed Wings at Speeds Below and Above the Speed of Sound," NACA TN 1032, March 1946, Langley Memorial Aeronautical Laboratory, Langley Field, Virginia.

10. DeYoung, J., "Rule of Thumb Equation for Predicting Lifting-Surface-Theory Values of Lift," Journal of the Aeronautical Sciences, Vol. 24, No. 8, August 1957, pp. 629.

11. McCormick, B.W., Aerodynamic of V/STOL Flight, Academic Press, New York, N.Y., 1967, pp. 45-48, 70.

12. Crooks, W.M., "A Fixed Vane Sensor for Measuring Turbulent Air Flows," Proceedings of the 10th National Aerospace Instrumentation Symposium, Instrument Society of America, New York, N.Y., 1964, 17 pp.

Appendix A

Computer Program

```
      PROGRAM A-BHDOT(INPUT,OUTPUT,TAPE5=INPUT,TAPE6=OUTPUT)
C
C     THIS PROGRAM IS WRITTEN IN FORTRAN EXTENDED AND WAS EXECUTED ON
C     THE CDC CYBER 74 COMPUTER AT WRIGHT-PATTERSON AFB,OHIO
C
      DIMENSION ALPHA(303),T(303),A(2),HDOTPLT(303),TEMP(4)
      COMMON HDOT0,IERNTRP,U,ZETA,WN,MUV,MUD,K,N,THDOT(10),HDOT(10),
     1  HDBLDOT,AFCTR
      REAL MUV,MUD,K,L,JNERTIA
C
C     PARAMETERS AND DATA ARE READ IN THE NEXT FOUR STATEMENTS.
C     VARIABLES AND APPROPRIATE UNITS ARE DEFINED IN THE WRITE FORMAT
C     STATEMENTS 940 AND 950.  THE DYNAMIC PARAMETERS ZETA AND FN
C     WILL BE GIVEN THEORETICAL VALUES IF NONE ARE READ. IF NOT
C     SPECIFIED, THE SOLUTION WILL START AT TIME=0 WITH AN INITIAL
C     VALUE OF HDBLDOT=0 USING A TIME STEP DELT=PERIOD/10.  INITIAL
C     CONDITIONS ON ALPHA AND ALPHADOT (A(1) AND A(2)) MUST BE
C     SPECIFIED (IN DEGREES).  THE NUMBER OF TIME STEPS IMAX IS LIMITED
C     TO 300 ALTHOUGH THIS COULD EASILY BE CHANGED PROVIDED LARGER
C     ARRAYS ARE SPECIFIED.  A TIME HISTORY OF THE PIVOT AXIS
C     VELOCITY HDOT MUST ALWAYS BE SPECIFIED (EVEN IF ZERO).
C     N SEQUENTIAL VALUES OF TIME AND THE CORRESPONDING HDOT ARE
C     READ STARTING WITH T(IME)HDOT.LE.INITIAL TIME.
C
      READ (5,900) CLALPHA,L,S,JNERTIA,B
      READ (5,910) Q,ZETA,MUV,MUD,K,FN
      READ (5,920) A(1),A(2),IMAX,DELT,TIME,HDBLDOT
      READ (5,930) N,(THDOT(J),HDOT(J),J=1,N)
      FNCNST=SQRT(CLALPHA*L*S/JNERTIA)/75.398
      FNTHRY=FNCNST*SQRT(Q)    $WNTHRY=6.2832*FNTHRY
      IF (FN.LE.0.)  FN=FNTHRY
      WN=6.2832*FN    $U=19.763*SQRT(Q)
      PERIOD=1./FN    $IF (DELT.LE.0.)  DELT=PERIOD/100
      ZETATHR=(2.*L*L+3.*L*B+B*B)/(4.*L)*WNTHRY/(U*17.6)
      ZETALMT=0.5*L*WNTHRY/(U*17.6)
      IF (ZETA.LE.0.)  ZETA=ZETATHR
C
C     IF THE SYSTEM IS OVERDAMPED, THE DAMPED PERIOD IS
C     ARTIFICIALLY REPORTED AS 99.99
C
      DMPRD=99.99
      IF (ZETA.LT.1.0)  DMPRD=PERIOD/SQRT(1.-ZETA**2)
      AFCTR=(2.*L+B)*B/(4.*L*U*17.6)
      T(1)=TIME    $ALPHA(1)=A(1)
      A(1)=A(1)/57.296    $A(2)=A(2)/57.296
C
C     INTERP IS A WPAFB LIBRARY SUBROUTINE BEING USED HERE AS A
C     LINEAR INTERPOLATOR TO OBTAIN A VALUE OF HDOT CORRESPONDING
C     TO THE SPECIFIED TIME.
C
      CALL INTERP(THDOT,HDOT,N,1,TIME,HDOTPLT(1),TEMP,IERNTRP)
      HDOTLST=HDOTPLT(1)
      IF (IMAX.GT.300)  IMAX=300
      IMAX1=IMAX+1
      DO 10 I=1,IMAX
C
```

```
C     RKDF IS A WPAFB LIBRARY ORDINARY DIFFERENTIAL EQUATION (O.D.E.)
C     SOLVER WHICH RETURNS A NEW VALUE OF A(LPHA) AND INCREMENTS TIME
C     USING A 4TH ORDER RUNGE-KUTTA SCHEME
C
      CALL RKDF(TIME,A,2,DELT,IERRK)
C
C     A SIMPLE FINITE DIFFERENCE APPROXIMATION IS USED TO ESTIMATE
C     THE PIVOT AXIS ACCELERATION HDBLDOT
C
      HDBLDOT=(HDOT0-HDOTLST)/DELT
      T(I+1)=TIME
      ALPHA(I+1)=A(1)*57.296
      HDOTLST=HDOTPLT(I+1)=HDOT0
C
C     NEXT STATEMENT PROTECTS AGAINST A DIVERGING SOLUTION
C
      IF (ABS(A(1)).GT.10.)  GO TO 20
   10 CONTINUE
   20 WRITE (6,940) Q,U,FN,WN,ZETA,MUV,MUD,K,PERIOD,DMPRD
      WRITE (6,950) CLALPHA,L,B,S,JNERTIA,FNCNST,FNTHRY,ZETATHR,ZETALMT
      WRITE (6,960) (T(I),ALPHA(I),HDOTPLT(I),I=1,IMAX1)
  900 FORMAT(5G10.3)
  910 FORMAT(6G10.3)
  920 FORMAT(2F5.0,I5,3G10.3)
  930 FORMAT(I5/(2G10.3))
  940 FORMAT("-DYNAMIC PRESSURE Q=",G11.4,"PSF.  EQUIVALENT (SEA-LEVEL)"
     1,"AIRSPEED U=",G11.4,"MPH."/" THE FOLLOWING PARAMETERS WERE THOSE
     2 ACTUALLY USED IN THE CALCULATED DYNAMIC RESPONSE..."/
     3" NATURAL FREQUENCY FN=",1PG11.4,"HZ. OR WN=",G11.4,"RAD/SEC."/
     4" AERO DAMPING ZETA=",G11.4," OTHER VISCOUS DAMPING COEFF MUSUBV="
     5,G11.4/" DRY FRICTION COEFF MUSUBD=",G11.4,"WITH STICTION FACTOR K
     6=",G11.4/" UNDAMPED PERIOD=",G11.4,"SEC.  DAMPED PERIOD=",G11.4,
     7"SEC."/"0INPUT AND THEORETICAL VALUES FOLLOW...")
  950 FORMAT("0CLALPHA=",G11.4,"  PIVOT TO C.P. DISTANCE L=",G11.4,"IN"/
     1" SEMI-CHORD B=",1PG11.4,"IN.  VANE AREA S=",G11.4,"IN**2"/
     2" VANE ASSEMBLY MASS MOMENT OF INERTIA J=",G11.4,"IN-LBF-SEC**2"/
     3" NATURAL FREQUENCY FN=",G11.4,"SQRT(Q) OR FN=",G11.4,"HZ."/
     4" DAMPING RATIO ZETA=",G11.4,"WHILE ITS LOWER LIMIT=",G11.4)
  960 FORMAT("0  TIME          ALPHA    AXIS HDOT"/3(1PG12.5))
      END
      SUBROUTINE F(T,A,ADOT)
C
C     THIS SUBROUTINE IS USED BY RKDF TO EVALUATE THE DERIVATIVES
C     A(LPHA)DOT OF A(LPHA) AT A SPECIFIED TIME T.
C
      DIMENSION A(2),ADOT(2),TEMP(4)
      COMMON HDOT(10),IERNTRP,U,ZETA,WN,MUV,MUD,K,N,THDOT(10),HDOT(10),
     1  HDBLDOT,AFCTR
      REAL MUV,MUD,K
      CALL INTERP(THDOT,HDOT,N,1,T,HDOT0,TEMP,IERNTRP)
C
C     THIS IS EQUATION 11 IN THE FORM OF 2 1ST ORDER O.D.E.'S
C
      ADOT(1)=A(2)
      ADOT(2)=-(WN**2)/(U*17.6)*(HDOT0+AFCTR*HDBLDOT)
     1  -(2.*ZETA*WN+MUV)*A(2)-(WN**2)*A(1)
     2  -MUD*SIGN(AMIN1(ABS(K*A(2)),1.0),A(2))
      RETURN
      END
```

```
                    0.785       0.665       11.28       0.001184   2.375
                    0.515       0.21        0.0         0.00       10.0        1.07
                    0.   0.0    300   0.00          0.000       0.0000
                      S
                    0.0         0.0
                    0.110       140.5
                    0.160        140.5
                    0.16001      0.0
                    10.0        0.0

DYNAMIC PRESSURE Q=   .5150     PSF.   EQUIVALENT (SEA-LEVEL)AIRSPEED U=  14.20 .  MPH.
THE FOLLOWING PARAMETERS WERE   THOSE   ACTUALLY USED IN THE CALCULATED DYNAMIC RESPONSE...
NATURAL FREQUENCY FN=   1.07      HZ. OR WN=   6.723      RAD/SEC.
AERO DAMPING ZETA=   .2100      OTHER VISCOUS DAMPING COEFF MUSUBV=   0.
DRY FRICTION COEFF MUSUBD=   0.          WITH STICTION FACTOR K=  10.00
UNDAMPED PERIOD=   .9346     SEC.   DAMPED PERIOD=   .9554     SEC.

INPUT AND THEORETICAL VALUES FOLLOW...

CLALPHA=  .7865     PIVOT TO C.P. DISTANCE L=  .6650     IN
SEMI-CHORD B=  2.375     IN.   VANE AREA S=  11.28     IN**2
VANE ASSEMBLY MASS MOMENT OF INERTIA J= 1.1643E-03IN-LBF-SEC**2
NATURAL FREQUENCY FN=  .9353     SQRT(K) OR FN=  .6712     HZ.
DAMPING RATIO ZETA= 7.1470E-  2WHICH IS LOWER LIMIT= 5.6122E-03

   TIME        ALPHA     AXIS ROOT
     0.          0.
 9.34579E-03-1.78886E-03  11.937
1.86916E-02-2.17933E-02  23.874
2.80374E-02-7.76422E-02  35.811
3.73832E-02  -.17884     47.749
4.67290E-02  -.33443     59.686
5.60748E-02  -.55321     71.623
6.54206E-02  -.84317     83.560
7.47664E-02 -1.2121      95.497
8.41121E-02 -1.6670      107.43
9.34579E-02 -2.2147      119.37
 .10280     -2.8613      131.31
 .11215     -3.6123      143.25
 .12150     -4.4676      140.50
 .13084     -5.4145      140.50
 .14019     -6.4413      140.50
 .14953     -7.5416      140.50
 .15888     -8.7094      140.50
 .16822     -9.8896      0.
 .17757     -10.912      0.
 .18692     -11.777      0.
 .19626     -12.574      0.
```

Sample data cards and partial output corresponding to one of the curves shown in Figure 21.

UNCLASSIFIED

SECURITY CLASSIFICATION OF THIS PAGE *(When Data Entered)*

REPORT DOCUMENTATION PAGE		READ INSTRUCTIONS BEFORE COMPLETING FORM
1. REPORT NUMBER AFIT TR 74-8	2. GOVT ACCESSION NO.	3. RECIPIENT'S CATALOG NUMBER
4. TITLE *(and Subtitle)* Dynamic Behavior of Angle-of-Attack Vane Assemblies		5. TYPE OF REPORT & PERIOD COVERED Final 6. PERFORMING ORG. REPORT NUMBER
7. AUTHOR(s) JAMES T. KARAM, JR. Captain, USAF		8. CONTRACT OR GRANT NUMBER(s)
9. PERFORMING ORGANIZATION NAME AND ADDRESS AFIT/ENM Wright-Patterson AFB, Ohio 45433		10. PROGRAM ELEMENT, PROJECT, TASK AREA & WORK UNIT NUMBERS
11. CONTROLLING OFFICE NAME AND ADDRESS		12. REPORT DATE December 1974 13. NUMBER OF PAGES 58
14. MONITORING AGENCY NAME & ADDRESS *(if different from Controlling Office)*		15. SECURITY CLASS. *(of this report)* UNCLASSIFIED 15a. DECLASSIFICATION/DOWNGRADING SCHEDULE

16. DISTRIBUTION STATEMENT *(of this Report)*

Approved for public release; distribution unlimited.

17. DISTRIBUTION STATEMENT *(of the abstract entered in Block 20, if different from Report)*

18. SUPPLEMENTARY NOTES

Report summarizing AFIT Faculty Research Project No 74-4.

19. KEY WORDS *(Continue on reverse side if necessary and identify by block number)*

Dynamic Model
Angle-of-Attack Vane
Wind Vane
Gust Measurement

20. ABSTRACT *(Continue on reverse side if necessary and identify by block number)*

A relatively simple analytic model was developed for predicting the dynamic behavior of angle-of-attack vane assemblies in response to changes in the free stream direction and/or to transverse motions of the vane's pivot axis. Experimental tests of a typical vane were performed in the AFIT five-foot, low subsonic wind tunnel. Comparisons were made of the model's predictions with these tests and with other test results found in the literature. The natural frequencies of the vanes were predicted reasonably well (within about 20 percent)

DD FORM 1 JAN 73 1473 EDITION OF 1 NOV 65 IS OBSOLETE

SECURITY CLASSIFICATION OF THIS PAGE *(When Data Entered)*

for all airspeeds -- subsonic and supersonic. The chief difficulty was in estimating the center of pressure location for these very low aspect ratio vanes. Viscous and tip effects were not included in the model. Viscous and tip effects were not included in the model. The aerodynamic damping was experimentally found to be essentially independent of airspeed as predicted, but the model's estimates were only within a factor of 2 to 3 of the data. It was found that typical aircraft instrumentation boom motions may lead to significant errors in the apparent angle of attack.

Additional Investigation of the Dynamic Behavior of Angle-of-Attack Vane Assemblies

A Supplement to AFIT TR-74-8
entitled "Dynamic Behavior of Angle-of-Attack
Vane Assemblies," dated December 1974

James T. Karam, Jr., Captain, USAF
Associate Professor of Aeronautical Engineering
Aero-Mechanical Engineering Department (AFIT/ENM)

May 1975

Approved for public release, distribution unlimited

Internal Working Document -- not an official Air Force Report

School of Engineering
Air Force Institute of Technology
Wright-Patterson Air Force Base, Ohio 45433

Table of Contents

Additional Nomenclature

C_i	ith capacitance; farad
e_i	voltage proportional to ith variable
s	Laplace variable
R_i	ith resistance; ohm
α	angle between vane and boom axis
β	angle between vane and effective free streams direction; $\alpha - \theta$
κ_α	vane assembly electronics gain; volts/deg
$\kappa_h^{\ddot{}}$	accelerometer electronics gain; volts/in/sec^2
θ	angle between effective free stream direction and boom axis
ω_b	break frequency associated with transverse acceleration; rad/sec

List of Additional Figures and Tables

Abstract

Additional release from an initial angle of attack tests were performed on a variety of windvane designs in the AFIT five-foot, low subsonic wind tunnel. Three basic construction types were investigated: all balsa, balsa/fiberglass sandwich, and Zytel (a tough plastic). An analytic model developed previously (AFIT TR 74-8) was further verified in that it reasonably predicted the effects of aspect ratio and moment of inertia changes. For the vanes tested, perforations were not found to have a significant effect on the damping ratio -- unlike the results of Lenschow. For use as a wind gust transducer in thunderstorm penetration studies, the Zytel vane with an aspect ratio of 0.5 in conjunction with signal conditioning is recommended. A specific conditioning design is suggested which, in conjunction with an accelerometer, should electronically cancel any erroneous output of the vane due to transverse motions of the aircraft instrumentation boom.

Introduction

Last year, an investigation into the dynamic behavior of angle-of-attack vane assemblies was performed in support of thunderstorm penetration studies being conducted by the 4950th Test Wing, Wright-Patterson AFB, Ohio. The resulting report [13,14] summarizes the development of a mathematical model of a vane and the model's verification by wind tunnel tests performed at AFIT and by other tests found in the literature. Based on the results of this prior study, some new vanes were designed which would hopefully have a better dynamic response. The current report summarizes the experimentally determined behavior of these new vane designs. In addition, these new designs allowed further verification of the mathematical model in that several additional parameters were varied. Finally, since none of the designs ameliorate the undesired response of the vane to plunging motions of the aircraft instrumentation boom, a signal conditioning design is included which should minimize these extraneous signals.

In order to avoid an unnecessary duplication of material, this document was not written to stand alone but as a supplement to the original study [13]. The figures, equations, tables, and references are numbered as a continuation of the original report. Much reference is made to material in the prior report as if it were a part of this current document, e.g., a reference to equation (11) which may be found in the original report.

Mathematical Model

In thunderstorm penetration studies, the vane assembly is not really used as an angle of attack indicator but is instead used to sense changes in the local free stream direction due to wind gusts. Figure 30 is a sketch of the coordinate system used for this study; it differs from Figure 2 only in that the free stream direction is no longer considered to be aligned with the axis of the boom. When used as a gust measurement device, the aircraft is in steady, level flight so that the boom axis may be considered fixed in space. The vane's synchro senses the angle α, and the mechanical rotary inertia term is proportional to $\ddot{\alpha}$. However, in a quasi-steady sense, the aerodynamic moments on the vane are proportional to $\beta = \alpha - \theta$ which is the angle between the effective free-stream direction and the vane. Neglecting the additional friction terms, equation (11) can be rewritten as

$$\ddot{\alpha} + 2\zeta\,\omega_n\,\dot{\beta} + \omega_n^2\,\beta = -\frac{\omega_n^2}{U}\left(\dot{h} + \frac{1}{\omega_b}\,\ddot{h}\right) \tag{39}$$

where

$$\omega_n = \sqrt{\frac{C_{L\alpha}\,\ell q\,s}{J}} = 2\,\pi\,f_n \tag{12}$$

$$\zeta = \frac{(2\ell^2 + 3\ell\,b + b^2)}{4\ell}\,\frac{\omega_n}{U} \tag{14}$$

$$\omega_b = \frac{4\ell}{2\ell + b}\,\frac{U}{b} \tag{40}$$

or, since $\beta = \alpha - \theta$

$$\ddot{\alpha} + 2\zeta\,\omega_n\,\dot{\alpha} + \omega_n^2\,\alpha = 2\zeta\,\omega_n\,\dot{\theta} + \omega_n^2\,\theta - \frac{\omega_n^2}{h}\left(\dot{h} + \frac{1}{\omega_b}\,\ddot{h}\right) \tag{41}$$

Converting to Laplace notation and considering the response of the vane to transverse accelerations of its pivot axis rather than displacements, since $\ddot{h}(s) = s^2\,h(s)$ and $\dot{h}(s) = sh(s) = \frac{1}{s}\,\ddot{h}(s)$, we have

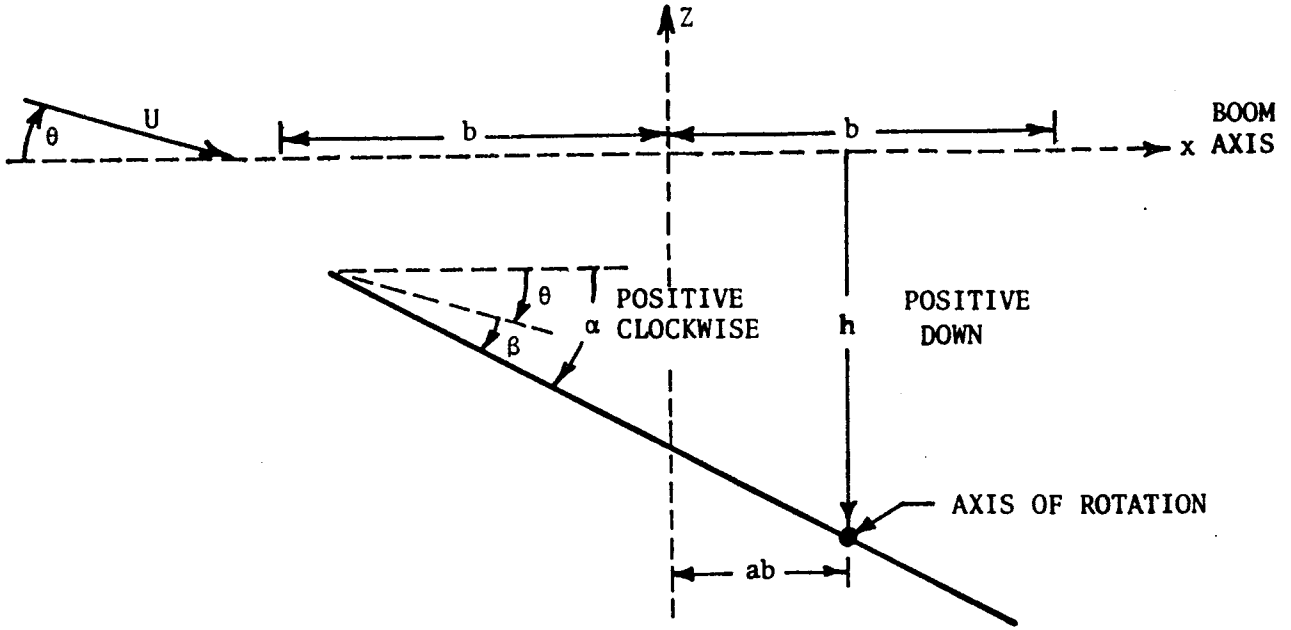

FIGURE 30 WINDVANE COORDINATE SYSTEM FOR VARIABLE FREESTREAM DIRECTION

$$(s^2 + 2\zeta\,\omega_n\,s + 1)\,\alpha(s) = (2\zeta\,\omega_n\,s + 1)\,\theta(s) - \frac{\omega_n^2}{U}\left(\frac{1}{s} + \frac{s}{\omega_b}\right)\ddot{h}(s)$$

or

$$\alpha(s) = \frac{1 + \dfrac{s}{\omega_n/2\zeta}}{1 + \dfrac{2\zeta}{\omega_n}s + \dfrac{s^2}{\omega_n^2}}\,\theta(s) - \frac{1 + \dfrac{s}{\omega_b}}{Us\left(1 + \dfrac{2\zeta}{\omega_n}s + \dfrac{s^2}{\omega_n^2}\right)}\,\ddot{h}(s) \qquad (42)$$

Thus, we find the angle of the vane with respect to the boom, α, may be considered as the response of a classical second order system to two inputs: the angle (and its derivatives) of the effective free stream direction with respect to the boom, θ, and the transverse accelerations, $\ddot{h}$, of the vane's pivot axis.

From a practical standpoint, there are two major problems with using such a vane to measure gusts in thunderstorms. First, the severe turbulence and hail encountered invariably excites the instrumentation boom into a bending oscillation. For the boom in current use on the F-4 test aircraft based at Oklahoma City, the first bending mode natural frequency was measured as 16 Hertz, and deflections estimated as large as $\pm$ 2 inches have been observed in flight. These figures would imply pivot axis accelerations of over 50 g's and could lead to vane deflections of $\pm$ 2 degrees at the typical aircraft penetration speed of 300 miles per hour. These vane deflections would be further increased if this exciting frequency were near the natural frequency of the vane since these vanes are typically lightly damped. Unfortunately, that is the case for the vanes in use for their natural frequency is about 15 Hertz, and the typical damping ratio of 0.2 could lead to more than double the angular deflection of the vane (see equation 38). Since the instrumentation boom cannot be made much stiffer, and a lower natural frequency of the vane would reduce its ability to respond to rapid gusts, a signal conditioning scheme is

suggested to obtain the desired response electrically. Figure 31 shows one possible conditioning scheme in block diagram form. First, the peaky underdamped second order term is cancelled by an identical numerator second order term. Then, the output of an accelerometer which is sensitive in the transverse direction is conditioned and subtracted from the vane signal so that the output is now only due to changes in the free stream direction, θ, and its derivative. Finally, a first order denominator term is used to provide an electrical output which is linearly proportional solely to θ for all frequencies. A specific electrical design for this conditioning circuit is suggested later in this report.

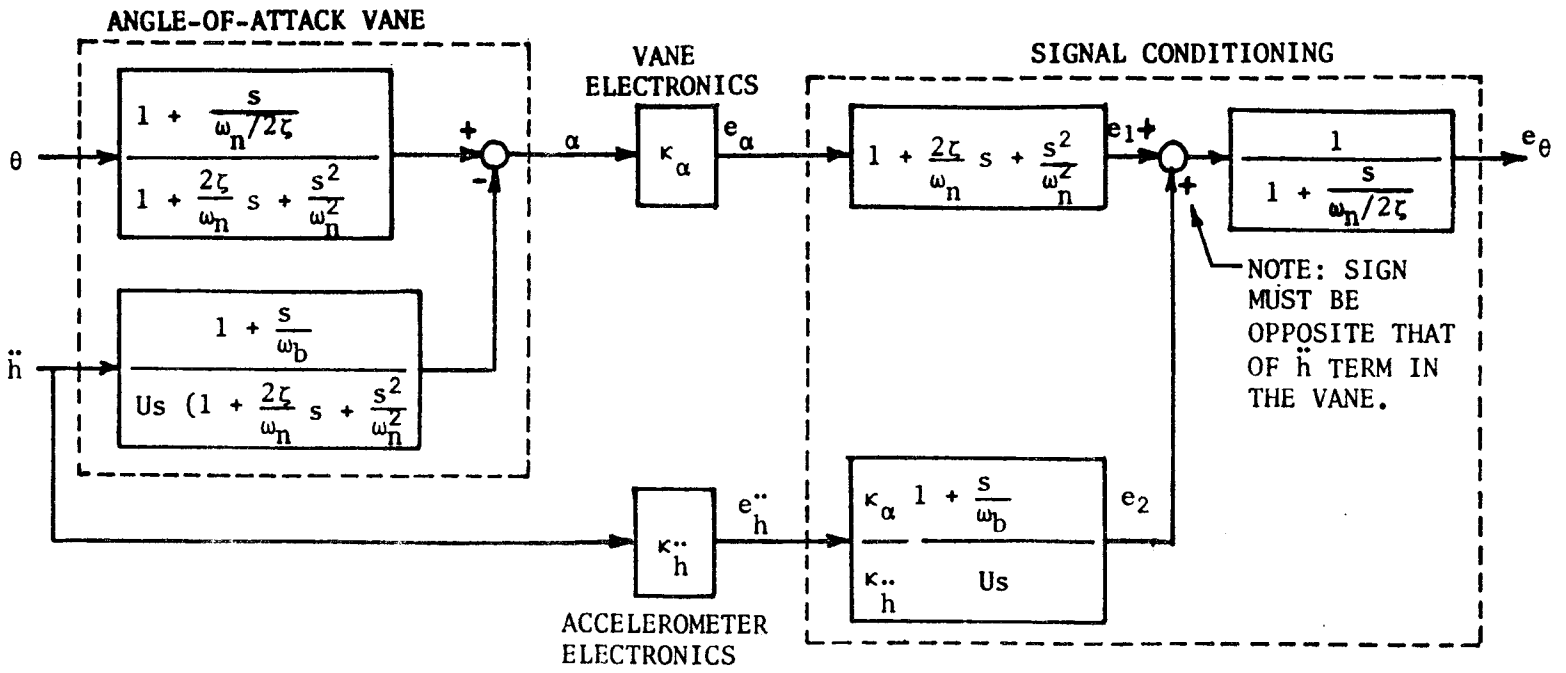

FIGURE 31 SYSTEM BLOCK DIAGRAM TO PROVIDE OUTPUT PROPORTIONAL ONLY TO CHANGES IN THE FREESTREAM DIRECTION

Experimental Program

Three basic types of vane construction were studied in the current series of wind tunnel tests: a balsa/fiberglass sandwich (see Figure 4), two thin ZYTEL (a tough plastic) sheets separated and stiffened by longitudinal ribs, and solid balsa stiffened by fiberglass cloth near the leading edge. Figure 33 is a photograph of some of the vanes tested. All vanes were thin ($\leq$ 1/8 inch thick), flat plates 4.75 inch long, 2.38 inch wide, which were pivoted about their leading edge as in Figure 4. Their aspect ratio was thus 0.5. Since the current design was known to be excited by boom vibration at near its natural frequency, a major design goal was to attempt to increase the damping ratio from its typical value of 0.2. Lenschow [5] had reported a doubling of the damping ratio by simply perforating the vane. Thus, solid vanes, and ones with 5/64 inch (2 mm) diameter holes, and 5/32 inch (4 mm) diameter holes were tested. The effect of chord length (and thus aspect ratio) was investigated by cutting off one of the Zytel vanes. Finally, although not tough enough to survive hail strikes in actual flight tests, the all balsa vane was tested to verify the effects of changes solely in moment of inertia. The inertias of each vane were measured by a torsional wire pendulum assembly.

All tests were performed by setting the vane at a small initial angle of attack and then releasing the vane by pulling a locking pin by means of a solenoid. The tunnel installation and a typical response are shown in Figures 5 and 6. The effective damping ratio was determined from the log decrement of adjacent extrema according to equation (23) and then the natural frequency from the observed damped period according to equation (26). The effect of initial amplitude was checked on the all balsa vane.

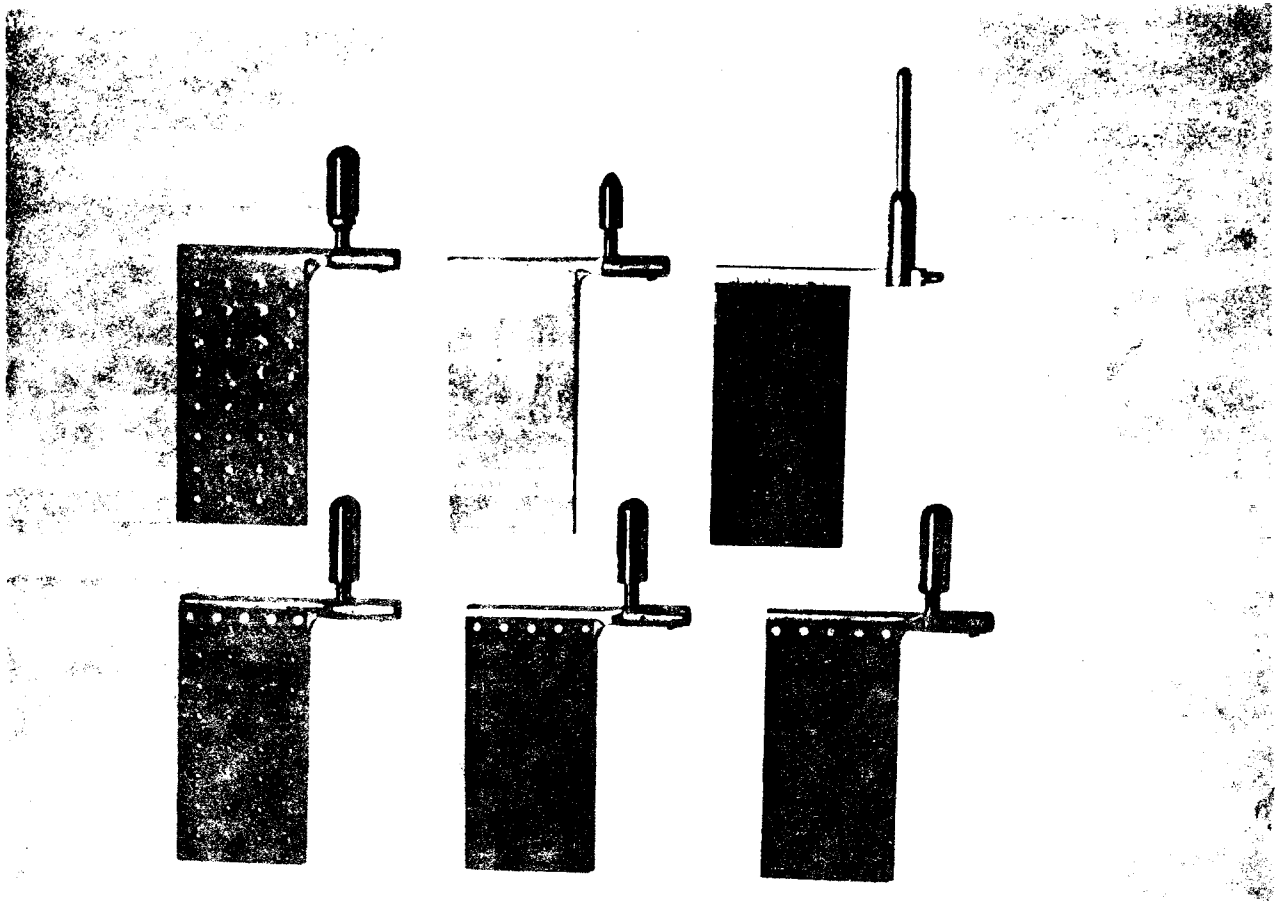

FIGURE 32 PHOTOGRAPH OF TYPICAL WINDVANES (BALSA/FIBERGLASS, ALL BALSA, ORIGINAL DESIGN IN TOP ROW; ZYTEL VANES IN BOTTOM ROW)

Comparison of Theory with Experiment

Figure 33 shows the experimental and theoretical values of the natural frequency and damping ratios of the balsa/fiberglass vane. This vane is basically the same as that originally tested except that the fiberglass core included some holes in an attempt to reduce the moment of inertia. Not much reduction was achieved (less than 10%), so the experimental results are essentially the same as before (compare Figure 33 with Figures 15 and 16). However, the test of Lenshow's vane perforation scheme did not produce the hoped for increase in damping. The hole sizes tested were the same (2mm) and double that found most effective by Lenshow [5]. As a possible explanation of this discrepancy, one can note that the inertia (and thus the forces) of this vane are almost two orders of magnitude larger than that of the vane tested by Lenschow. Thus, while the viscous forces due to flow through small holes may have been significant for Lenschow's small vane, their effect is apparently negligible on vanes of the size tested herein.

Perforation similarly had a negligible effect on the response of the Zytel vanes as may be seen in Figure 34. Since the Zytel and balsa/fiberglass vanes have similar geometry and inertias, their dynamic behavior is essentially the same. As before, some effects (probably) due to dry friction are noted at the very small airspeeds, but the damping ratio is essentially constant for air speeds on the order of 100 mph or greater, while the natural frequency increases linearly with equivalent airspeed.

The effect of reducing the chord length (and thus increasing the aspect ratio) of the Zytel vanes is shown in Figure 35. Here, as in the other figures, the theoretical lines are predicted by equation (12) for

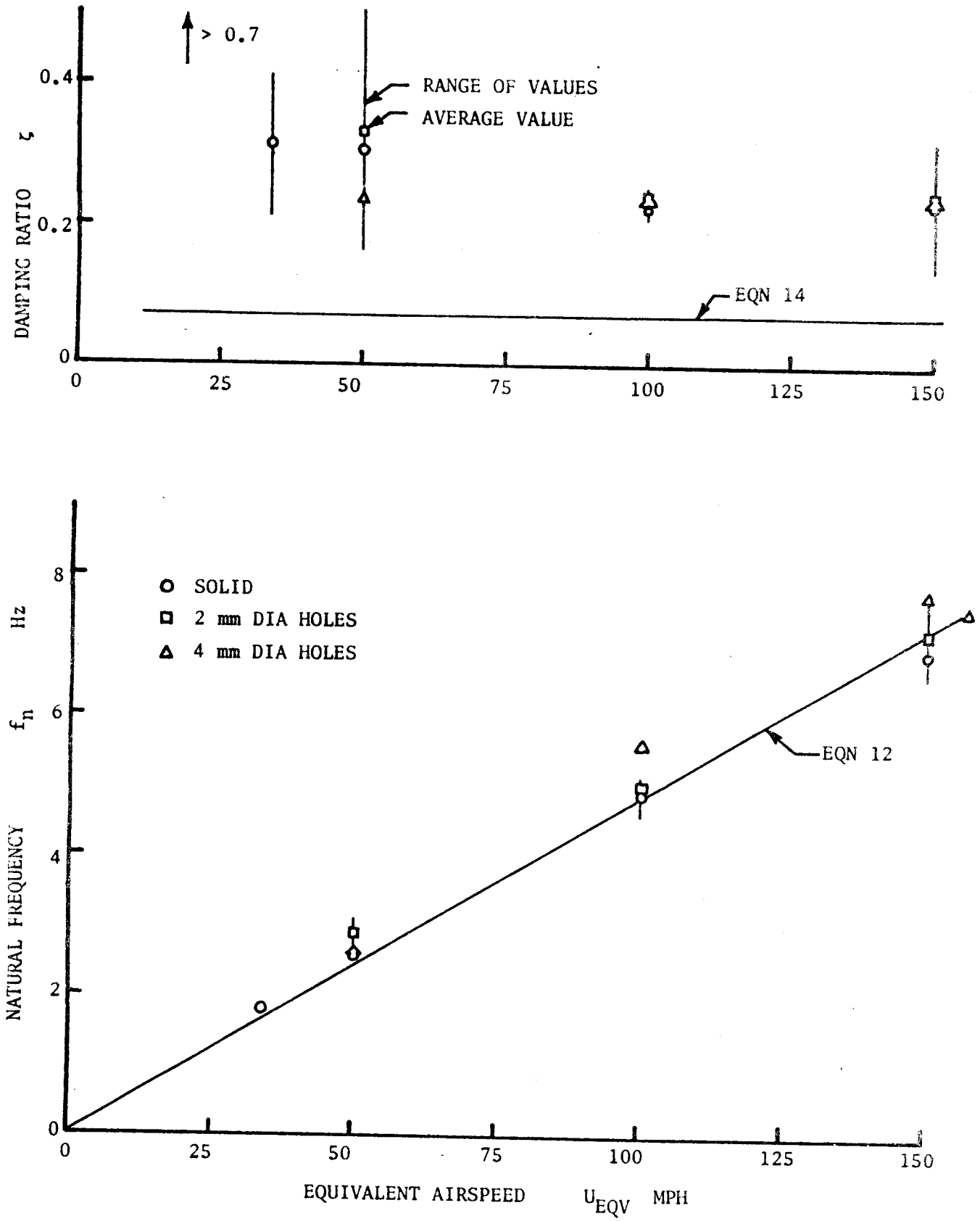

FIGURE 33 EFFECT OF PERFORATIONS ON DYNAMIC RESPONSE OF BALSA/FIBERGLASS VANES WHOSE ASPECT RATIO IS 0.5

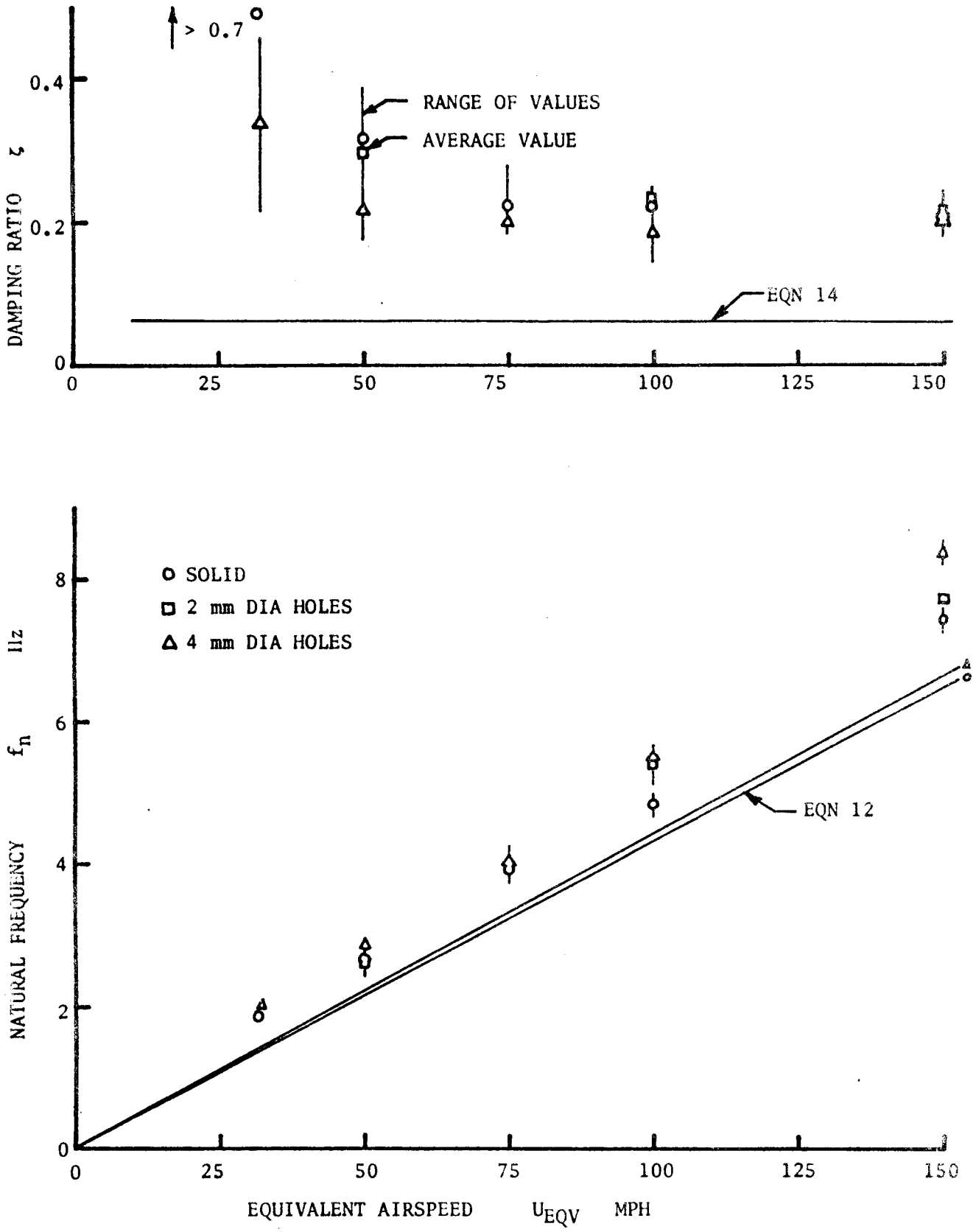

FIGURE 34 EFFECT OF PERFORATIONS ON DYNAMIC RESPONSE OF ZYTEL VANES WHOSE ASPECT RATIO IS 0.5

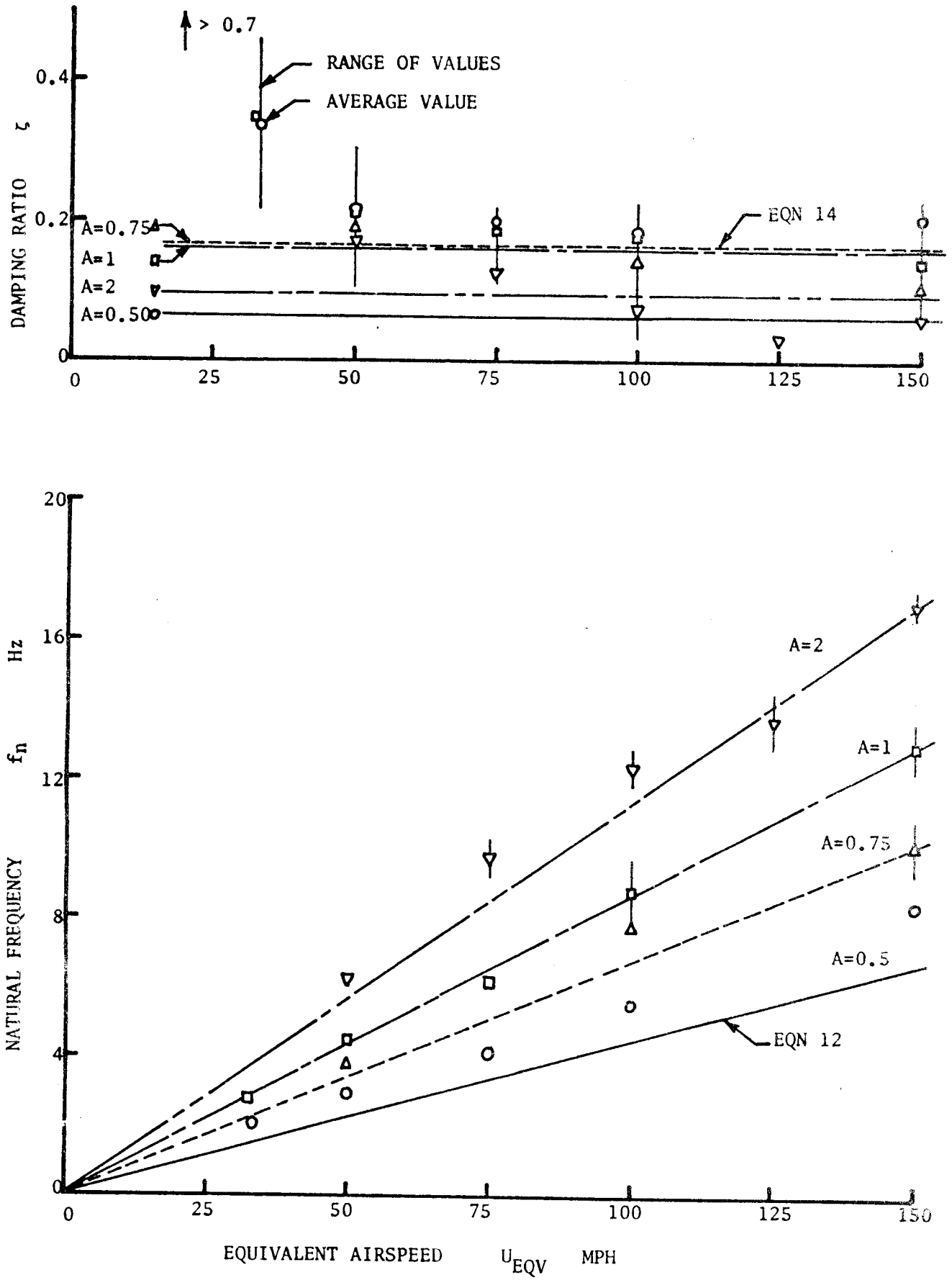

FIGURE 35 EFFECT OF CHORD LENGTH (ASPECT RATIO) ON DYNAMIC RESPONSE OF ZYTEL VANES

natural frequency and equation (14) for the damping ratio. Measured values for moment of inertia J (including counterweight), planform area S, semi-chord b, and dynamic pressure q, were used in conjunction with theoretical values for lift curve slope $C_{L\alpha}$ from equation (21) and the center of pressure location ℓ from Figure 14 to perform the calculations. As may be noted, the effects of aspect ratio are reasonably predicted by the theory.

While the reduction in chord also reduces the inertia of the Zytel vane, the effect of an inertia change alone was investigated with an all balsa vane which is geometrically identical to the balsa/fiberglass vane. As may be seen in Figure 36, this fourfold reduction in inertia does indeed cause a doubling in both the natural frequency and damping as predicted. It is also apparent from the observed damping that dry friction effects are significant at higher airspeeds than before -- again as expected. Finally, the effects of initial amplitude were investigated with this vane. While the other tests were conducted with an initial amplitude of about 3 degrees, amplitudes of about half and double this value were also tested in the balsa vane. The largest amplitude (about 6 degrees) appears to lead to a natural frequency about 10% higher than do the smaller amplitude values. This increase in natural frequency could possibly be explained by the non-linearly increasing lift coefficient with increasing angle of attack for these low aspect ratio airfoils (see Figure 5 of Gersten [7]). However, such an increase in lift coefficient should also manifest itself in an increase in the damping ratio, but such was not noted. In fact, the effective damping ratio decreases with increasing amplitude. The observed damping behavior is a trait of dry friction as discussed earlier (see Figure 18).

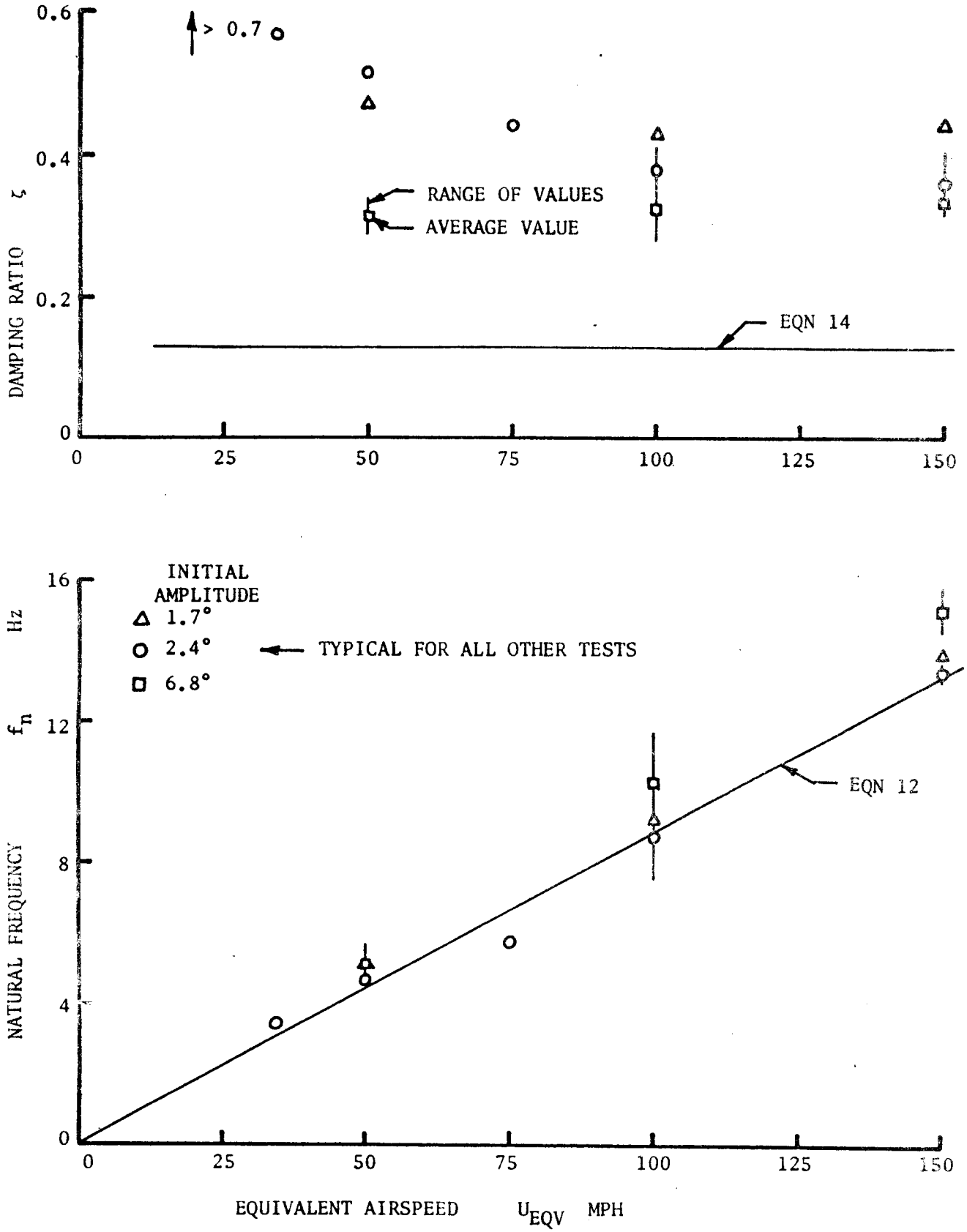

FIGURE 36 EFFECT OF INITIAL AMPLITUDE ON THE DYNAMIC RESPONSE OF ALL-BALSA VANE WHOSE ASPECT RATIO IS 0.5

Table IV summarizes the results of the supplemental test program. Listed are the configurations, moments of inertia, and average experimental values for natural frequency (expressed as $f_n/\sqrt{q}$ where q is in psf) and damping ratio (using values only for airspeeds of 100 mph and greater in an attempt to estimate just the aerodynamic damping). Also listed are the values of moment coefficient $C_{L\alpha}\ \ell$ inferred from the measured natural frequency in comparison with the theoretical values obtained from equation (21) and Figure 14. The difference between these theory and inferred values would represent an average error of + 7.2% with a standard deviation of 8.0% in the predicted natural frequency of the tests of Zytel vanes as aspect ratio was varied. Similarly, the average disagreement in the natural frequency prediction for all the vanes with an aspect ratio of 0.5 was + 12.4% with a standard deviation of 7.4%. The observed damping ratio was again about 3 times that predicted by equation (14) for all vanes with an aspect ratio of 0.5. The larger aspect ratio vanes showed much less disagreement. It should be noted that the observed values of damping are still 20 to 50 times larger than the estimate provided by equation (18) which has appeared previously in the literature.

Table IV Summary of Results of Supplemental Tests

Material	Configuration A	Hole Dia	J in lb_f sec^2	$f_n/\sqrt{q}$ cps/$\sqrt{psf}$	$C_{L\alpha}{}^{\ell}$ inferred	$C_{L\alpha}{}^{\ell}$ theory	ζ exp	$\frac{\zeta_{exp}}{\zeta_{eqn\ 14}}$
ZYTEL	0.5	SOLID	0.00137	1.009	0.702	0.509	0.216	3.4
ZYTEL	0.5	2 mm	0.00139	1.041	0.759	0.509	0.227	3.6
ZYTEL	0.5	4 mm	0.00131	1.116	0.822	0.509	0.196	3.0
ZYTEL	0.75	SOLID	0.000468	1.474	0.768	0.639	0.161	1.0
ZYTEL	1.0	SOLID	0.000205	1.694	0.593	0.615	0.166	1.0
ZYTEL	2.0	SOLID	0.000061	2.379	0.696	0.626	0.059	0.6
BALSA/FBGLS	0.5	SOLID	-	0.968	-	-	0.228	-
BALSA/FBGLS	0.5	2 mm	-	1.006	-	-	0.246	-
BALSA/FBGLS	0.5	4 mm	0.00110	1.047	0.608	0.509	0.234	3.3
BALSA	0.5	SOLID	0.000322	1.861	0.562	0.509	0.368	2.8

Design Considerations

For the thunderstorm application to which this study was directed, the solid Zytel vane with an aspect ratio of 0.5 seems the most appropriate. For the same size, it has essentially the same dynamic behavior as the balsa/fiberglass vane but should prove much tougher against damage due to hail. While one can raise the natural frequency by reducing the chord and thus the inertia, the resulting damping is less. Further, the shorter chord Zytel vanes showed an increase in the "steady state" dither -- possibly due to unsteady vortex shedding from their blunt trailing edges. The peak-to-peak value of this "steady state" noise increased from about $\pm$ 0.1 degrees to about $\pm$ 0.5 degrees as the aspect ratio was varied from 0.5 to 2. This noise might be reduced by tapering the Zytel vanes, but only additional tests could verify this; and the damping would still be less. Reducing inertia only (as with the all balsa vane) does improve both damping and natural frequency, but it also allows dry friction to remain significant at higher airspeeds and amplitudes. With the currently available synchros and shaft bearings, even if an ultralight but tough material became available, it is doubtful that one could raise the natural frequency to get it so far removed from the support boom's oscillation frequency that one could avoid signal conditioning. Further, if one must signal condition, it makes more sense to use a "poor" performing vane with a low natural frequency and damping but which behaves linearly than to use a "better" vane whose dynamic performance is dominated by nonlinear dry friction effects. It is much more difficult, if not impossible, to cancel a nonlinear undesired behavior than to cancel a linear undesired behavior.

Earlier in this report (see Figure 31), a signal conditioning approach was suggested. In this section, one possible hardware design based on operational amplifiers will be developed to implement the scheme. First, some general designs are proposed to perform each conditioning function, and then specific components are selected for a vane and operating conditions typical of the actual flight test aircraft. The electrical designs are shown in Figure 37. A good reference for op amp based circuit design is the text by Korn and Korn [15].

The upper circuit of Figure 37 can provide the desired numerator second order term. Note that such a circuit may need to be preceded by a low-pass filter since it is a noise enhancer. Based on the circuits summarized in Appendix A of [15], it's transfer function in Laplace notation is

$$\frac{e_1}{e_\alpha} = -\frac{2R_2\ (1 + \frac{1}{2} R_2\ C_3\ s)}{2R_1\ (1 + \frac{1}{2} R_1\ C_1\ s)} \Big/ \frac{}{1 + 2R_1\ C_2\ s + R_1^2\ C_1\ C_2\ s^2} = -\left(1 + \frac{2\zeta}{\omega_n} s + \frac{s^2}{\omega_n^2}\right) \qquad (43)$$

provided we set

$$R_1 = R_2 \qquad (44a)$$

$$C_1 = C_3 \qquad (44b)$$

$$2R_1\ C_2 = 2\zeta/\omega_n \qquad (44c)$$

$$R_1^2\ C_1\ C_2 = 1/\omega_n^2 \qquad (44d)$$

The middle circuit of Figure 37 can properly condition the accelerometer output. Its transfer function is

$$\frac{e_2}{e_h''} = -\frac{\frac{R_4}{1 + R_4\ C_5\ s}}{\frac{R_3}{1 + R_3\ C_4\ s}} = -\frac{\frac{R_4}{R_3}\ (1 + R_3\ C_4\ s)}{1 + R_4\ C_5\ s} \propto -\frac{\kappa_\alpha}{\kappa_h''} \frac{\left(1 + \frac{s}{\omega_b}\right)}{Us} \qquad (45)$$

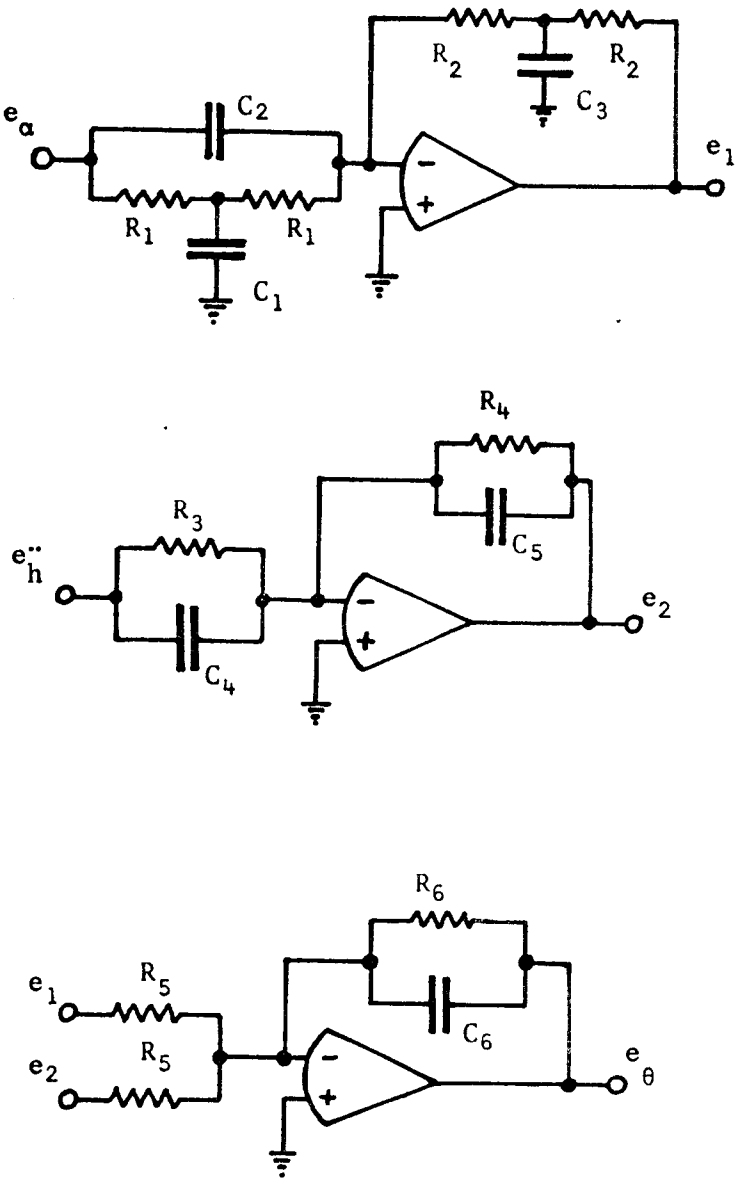

FIGURE 37 A POSSIBLE DESIGN FOR SIGNAL CONDITIONING

provided we set

$$R_4 = R_3 \tag{46a}$$

$$R_3\, C_4 = 1/\omega_b \tag{46b}$$

$$R_4\, C_5 = \kappa_{\ddot{h}}\, U/\kappa_\alpha \tag{46c}$$

The approximation in equation (45) is necessary to preclude saturation of the op amp. Finally, the lower circuit will act as a summer and a denominator first order since its transfer function is

$$e_\theta = \frac{\dfrac{-R_6}{1 + R_6\, C_6\, s}}{R_5}\, e_1 + \frac{\dfrac{-R_6}{1 + R_6\, C_6\, s}}{R_5}\, e_2 \tag{47}$$

or

$$\frac{e_\theta}{e_1 + e_2} = -\frac{R_6/R_5}{1 + R_6\, C_6\, s} = -\frac{1}{1 + \dfrac{s}{\omega_n/2\zeta}} \tag{48}$$

provided

$$R_5 = R_6 \tag{49a}$$

$$R_6\, C_6 = 2\zeta/\omega_n \tag{49b}$$

As an example of a specific design, consider a solid Zytel vane on the test aircraft penetrating at 300 mph. The significant parameters are then

$$U = 300 \text{ mph} = 5280 \text{ in/sec},\ b = 2.375 \text{ in, and } \ell = 0.655 \text{ in.}$$

Then from extrapolating Figure 34, we find

$$f_n \simeq 15 \text{ Hz} \quad \text{or} \quad \omega_n \simeq 94 \text{ rad/sec} \quad \text{and} \quad \zeta \simeq 0.2.$$

The aircraft test electronics is such that

$$\kappa_\alpha = 0.25 \text{ volts/deg} = 14.32 \text{ volts/radian and}$$

$$\kappa_{\ddot{h}} = 0.25 \text{ volts/g} = 0.000647\ \frac{\text{volts}}{\text{in/sec}^2}$$

Then

$$\frac{\omega_n}{2\zeta} = 236\ \frac{\text{rad}}{\text{sec}},\ \frac{\kappa_\alpha}{\kappa_{\ddot{h}} U} = 0.00128\ \frac{\text{rad}}{\text{sec}},\ \text{and } \omega_b = \frac{4\ell}{2\ell + b}\,\frac{U}{b} = 1580\ \frac{\text{rad}}{\text{sec}}.$$

As with most op amp designs, at least one component value may be selected arbitrarily. Because of the relatively low frequencies involved in this system, relatively large capacitances are needed. However, the use of nonpolarized tantalum capacitors will minimize the physical size of the components. Further, for proper functioning of the op amp, one needs to require that all resistances be on the order of one megohm or less.

With these points in mind, for the upper circuit of Figure 37, one may arbitrarily set $C_1 = C_3 = 10^{-6}$ farad = 1μf. Then satisfying the other parts of equations (44), in particular (44d) states

$$R_1^2 C_1 C_2 = \frac{1}{\omega_n^2}$$

or $$R_1 (R_1 C_2) = \frac{1}{\omega_n^2 C_1}$$

but eqn (44c) is $2R_1 C_2 = 2\zeta/\omega_n$

so 44a and 44d become $R_2 = R_1 = \frac{1}{\zeta \omega_n C_1} = \frac{1}{(0.2)(94)(10^{-6})} = 53000$ ohm = 53KΩ

Finally, $$C_2 = \frac{\zeta}{R_1 \omega_n} = \frac{0.2}{(53000)(94)} = 4.10^{-8} \text{ farad} = 0.04 \text{ μf.}$$

For the middle circuit of Figure 37, if one arbitrarily sets $C_5 = 10^{-3}$ farads = 1000 μf, then equation (46a) and (46c) requires

$$R_3 = R_4 = (\kappa_h'' U/\kappa_\alpha)/C_5 = \frac{1}{(0.00128)(10^{-3})} = 780000 \text{ ohm} = 780 \text{ KΩ}$$

Satisfying the above relation is the most important since the transverse motion cancellation is the most critical conditioning function. Finally, equation (46b) requires

$$C_4 = \frac{1}{R_4 \omega_b} = \frac{1}{(780000)(1580)} = 8.1 \cdot 10^{-10} \text{ farad} = 0.00081 \text{ μf} = 810 \mu\mu\text{f}$$

For the lower circuit, arbitrarily setting $C_6 = 10^{-7}$ farad = 0.1 μf, then equation (49) leads to

$$R_5 = R_6 = \frac{2\zeta}{\omega_n} / C_6 = \frac{1}{(236)(10^{-7})} = 42000 \text{ ohm} = 42 \text{ K}\Omega.$$

In summary, one possible implementation of the signal conditioning scheme of Figure 31 with the electrical circuits of Figure 37 will result from the components listed below when used with a solid Zytel vane on the test aircraft flying at 300 mph.

C_1 = 1 μf	R_1 = 53 KΩ
C_2 = 0.04 μf	R_2 = 53 KΩ
C_3 = 1 μf	R_3 = 780 KΩ
C_4 = 810 μμf	R_4 = 780 KΩ
C_5 = 1000 μf	R_5 = 42 KΩ
C_6 = 0.1 μf	R_6 = 42 KΩ

Conclusions and Recommendations

1. The analytic model developed in the original study [13] was experimentally verified further by varying the chordlength (thus, aspect ratio) and the moment of inertia. As before, the natural frequency was predicted within 10-20%, and the damping ratio was found to be independent of airspeed. While the observed damping was about 3 times that predicted for all vanes with an aspect ratio of 0.5, the other aspect ratios showed better agreement.

2. Unlike Lenschow's results [5], vane perforations did not have any significant effect on the dynamic behavior for vanes of the size tested herein.

3. A solid Zytel vane of aspect ratio equal to 0.5 in conjunction with signal conditioning is recommended for flight test. This vane has a reasonably good dynamic behavior ($f_n \approx 15$ Hz at 300 mph, $\zeta \approx 0.2$), is tough enough to survive hail, and has a linear behavior. The signal conditioning in conjunction with an independent measurement of transverse acceleration can provide an output which is almost solely due to changes in the effective free stream direction due to gusts.